NASA/TP-2000-210549

Bending Boundary Layers in Laminated-Composite Circular Cylindrical Shells

Michael P. Nemeth and Stanley S. Smeltzer, III
Langley Research Center, Hampton, Virginia

November 2000

The NASA STI Program Office . . . in Profile

Since its founding, NASA has been dedicated to the advancement of aeronautics and space science. The NASA Scientific and Technical Information (STI) Program Office plays a key part in helping NASA maintain this important role.

The NASA STI Program Office is operated by Langley Research Center, the lead center for NASA's scientific and technical information. The NASA STI Program Office provides access to the NASA STI Database, the largest collection of aeronautical and space science STI in the world. The Program Office is also NASA's institutional mechanism for disseminating the results of its research and development activities. These results are published by NASA in the NASA STI Report Series, which includes the following report types:

- TECHNICAL PUBLICATION. Reports of completed research or a major significant phase of research that present the results of NASA programs and include extensive data or theoretical analysis. Includes compilations of significant scientific and technical data and information deemed to be of continuing reference value. NASA counterpart of peer-reviewed formal professional papers, but having less stringent limitations on manuscript length and extent of graphic presentations.

- TECHNICAL MEMORANDUM. Scientific and technical findings that are preliminary or of specialized interest, e.g., quick release reports, working papers, and bibliographies that contain minimal annotation. Does not contain extensive analysis.

- CONTRACTOR REPORT. Scientific and technical findings by NASA-sponsored contractors and grantees.

- CONFERENCE PUBLICATION. Collected papers from scientific and technical conferences, symposia, seminars, or other meetings sponsored or co-sponsored by NASA.

- SPECIAL PUBLICATION. Scientific, technical, or historical information from NASA programs, projects, and missions, often concerned with subjects having substantial public interest.

- TECHNICAL TRANSLATION. English-language translations of foreign scientific and technical material pertinent to NASA's mission.

Specialized services that complement the STI Program Office's diverse offerings include creating custom thesauri, building customized databases, organizing and publishing research results . . . even providing videos.

For more information about the NASA STI Program Office, see the following:

- Access the NASA STI Program Home Page at *http://www.sti.nasa.gov*

- Email your question via the Internet to help@sti.nasa.gov

- Fax your question to the NASA STI Help Desk at (301) 621-0134

- Telephone the NASA STI Help Desk at (301) 621-0390

- Write to:
  NASA STI Help Desk
  NASA Center for AeroSpace Information
  7121 Standard Drive
  Hanover, MD 21076-1320

NASA/TP-2000-210549

Bending Boundary Layers in Laminated-Composite Circular Cylindrical Shells

Michael P. Nemeth and Stanley S. Smeltzer, III
Langley Research Center, Hampton, Virginia

National Aeronautics and
Space Administration

Langley Research Center
Hampton, Virginia 23681-2199

November 2000

Dedication

Dedicated to Professor J. Lyell Sanders, Jr., a former employee of NASA Langley Research Center, for his profound contributions to shell theory.

Available from:

NASA Center for AeroSpace Information (CASI)
7121 Standard Drive
Hanover, MD 21076-1320
(301) 621-0390

National Technical Information Service (NTIS)
5285 Port Royal Road
Springfield, VA 22161-2171
(703) 605-6000

Summary

An analytical, parametric study of the attenuation of bending boundary layers or edge effects in balanced and unbalanced, symmetrically and unsymmetrically laminated thin cylindrical shells is presented for nine contemporary material systems. The analysis is based on the linear Sanders-Koiter shell equations and specializations to the Love-Kirchhoff shell equations and Donnell's equations are included. Two nondimensional parameters are identified that characterize and quantify the effects of laminate orthotropy and laminate anisotropy on the bending boundary-layer decay length in a very general and encompassing manner.

A substantial number of structural design technology results are presented for a wide range of laminated-composite cylinders. For all laminate constructions considered, the results show that the differences between results that were obtained with the Sanders-Koiter shell equations, the Love-Kirchhoff shell equations, and Donnell's equations are negligible. The results also show that the effect of anisotropy in the form of coupling between pure bending and twisting has a negligible effect on the size of the bending boundary-layer decay length of the balanced, symmetrically laminated cylinders considered. Moreover, the results show that coupling between the various types of shell anisotropies has a negligible effect on the calculation of the bending boundary-layer decay length in most cases. The results also show that, in some cases, neglecting the shell anisotropy results in underestimating the bending boundary-layer decay length and, in other cases, results in an overestimation. An example problem is included in an appendix that demonstrates how to perform the calculations that were used to generate the results of the present study.

Symbols

a_{12}, a_{22}, a_{26}, b_{21}	inverted stiffness expressions defined in appendix C
$\bar{a}_{12}$, $\bar{a}_{22}$, $\bar{a}_{26}$, $\bar{b}_{21}$	modified inverted stiffness expressions defined in appendix B
$\mathcal{A}$, $\mathcal{A}_0$	nondimensional anisotropy parameters
A_{11}, A_{12}, A_{16}, A_{22}, A_{26}, A_{66}	laminate membrane stiffnesses
$\bar{A}_{16}$, $\bar{A}_{26}$, $\bar{A}_{66}$	modified laminate stiffnesses defined in appendix B
B_{11}, B_{12}, B_{16}, B_{22}, B_{26}, B_{66}	laminate membrane-bending coupling stiffnesses
$\bar{B}_{16}$, $\bar{B}_{26}$	modified laminate stiffnesses defined in appendix B
$\mathcal{C}_1$	first-order correction factor for anisotropy parameter
d, d^o	attenuation or decay lengths for which anisotropy is included and neglected, respectively
D_{11}, D_{12}, D_{16}, D_{22}, D_{26}, D_{66}	laminate bending stiffnesses
e, e_0	stiffness coefficients defined in appendixes C and B, respectively

E_1, E_2	major and minor principal lamina moduli, respectively
G_{12}	lamina shear modulus
h, L	cylinder wall thickness and length, respectively
M_x, M_θ, $M_{x\theta}$	axial and circumferential bending and twisting stress resultants, respectively
N_x, N_θ, $N_{x\theta}$	axial, circumferential, and shear membrane stress resultants, respectively
$\mathcal{O}$	nondimensional orthotropy parameter
P(x)	loading function appearing in bending boundary-layer differential equation
Q, S, T	constant coefficients of bending boundary-layer differential equation
Q_x, Q_θ	axial and circumferential transverse-shear stress resultants, respectively
R	cylinder radius
$\hat{T}$	modified shear stress resultant defined in appendix B
$\mathcal{U}$	strain-energy density
w	radial-displacement component
x	axial coordinate of cylinder
ε	attenuation-length tolerance parameter
ε_x^o, ε_θ^o, $\gamma_{x\theta}^o$	axial, circumferential, and shear membrane strains, respectively
θ	circumferential, angular coordinate
κ_x^o, κ_θ^o, $\kappa_{x\theta}^o$	axial and circumferential bending and twisting strains, respectively
μ	constant defining different shell theories
ν_{12}	lamina major Poisson's ratio
ϕ	lamina fiber angle (see fig. 4)

Introduction

The term, "bending boundary layer," refers to localized zones of bending stresses and deformations that appear in practically every type of thin-shell structure (ref. 1). Bending boundary layers are caused by edge support conditions; by localized mechanical loads, heating, or cooling; and by abrupt changes in stiffness, such as those caused by a cutout, a crack, or a stiffener. All these effects may be real concerns in a given preliminary design for an advanced aerospace vehicle made of laminated-composite materials. Thus, it is useful to have nondimensional parameters that characterize the effects of shell

geometry and laminate orthotropy and anisotropy on the extent of bending boundary layers that can be used to help guide the development of a design. For example, an optimal design for a pressure vessel might be one that exploits the membrane load-carrying action of a shell and minimizes zones of local bending stresses. Meaningful nondimensional parameters could be used at the preliminary design stage to identify families of laminates and material systems that exhibit relatively small bending boundary layers. Moreover, a meaningful estimate of the size of a bending boundary layer in a shell is very useful for determining an adequate first-approximation finite-element model for a complex shell structure. Without a proper understanding of the extent of a bending boundary layer, it is possible to have a finite-element model that could miss a significant part of the structural response in a region where failures are often initiated by high interlaminar stresses. Furthermore, a priori knowledge of the extent of bending boundary layers is useful in determining the instrumentation locations in structural verification tests and in material characterization tests (ref. 2). In addition, knowledge of how laminate construction affects the extent of a bending boundary layer is useful for understanding how nonlinear prebuckling deformations affect the buckling behavior of cylindrical shells.

Studies of the behavior of axisymmetric, bending boundary layers in right-circular, cylindrical shell structures made of orthotropic or anisotropic materials and with finite length have been presented, to at least some extent, in references 1 through 13. In the discussion that follows, reference is made to unbalanced and balanced laminates that are either symmetrically or unsymmetrically laminated. Herein, the term unbalanced laminate is used to indicate that coupling between pure extension or contraction and shearing is present in a laminate. The term unsymmetric laminate is used to indicate coupling between any of the components of bending action with any of the components of membrane action. A fully anisotropic laminate would include both these types of anisotropy, in addition to the anisotropy that is manifested by coupling between pure bending and twisting action that is sometimes exhibited by balanced, symmetric laminates.

In reference 1, an analysis is presented, and an expression for the attenuation or decay length of the bending boundary layer for a specially orthotropic cylinder that is subjected to edge loads, internal pressure, and heating is given. These equations, and the accompanying results, are based on the linear Love-Kirchhoff shell equations. In reference 3, an analytical solution that is based on Donnell's simplifications to the linear Love-Kirchhoff shell equations is given for fully anisotropic cylinders that are subjected to lateral pressure and edge loads. Results that show the effect of laminate anisotropy on the edge moment are presented for a clamped two-ply shell that is subjected to internal pressure. In addition, a discussion is presented that suggests that solutions based on Donnell's equations should be accurate for laminates that are not highly anisotropic. An analytical study of bending boundary layers in unbalanced, symmetrically laminated cylinders, which is also based on Donnell's equations, is presented in reference 2. The aim of this study was to determine a suitable gage section in a laminated-composite tube that is to be used for a material characterization test. Results are presented for unidirectional, helical-wound tubes.

An analytical solution for bending boundary layers in unbalanced, symmetrically laminated and balanced, unsymmetrically laminated circular cylindrical shells that are subjected to internal pressure and thermal loads is presented in reference 4. The solution is also based on Donnell's linear equations, and numerical results are presented for filament-wound cylinders made of heat-treated carbon-carbon material. A study that focuses mainly on prebuckling deformations, with bending boundary layers, in homogeneous, orthotropic and unsymmetrically laminated cross-ply cylinders that are subjected to axial-compression loads and lateral pressure loads is presented in reference 5. The effects of the bending boundary layers on the buckling response are examined for several laminate constructions, but the general effects of the laminate construction on the extent of the boundary layers are not discussed.

A pair of complex conjugate, fourth-order equations that are based on Flugge's corresponding equations (ref. 14), which can be solved in closed form, are derived for specially orthotropic, circular cylindrical shells in reference 6. Moreover, eigenfunction solutions are presented that include the solution for the axisymmetric bending boundary layer; several simplified equations are presented and their relative accuracy is analyzed. In reference 7, a study of bending boundary layers in transversely isotropic circular cylindrical shells is presented. This study examines the attenuation characteristics of bending boundary layers by applying an asymptotic method to the linear, three-dimensional elasticity equations and presents order-of-magnitude estimates for the stresses and displacements for a wide range of ratios of the two principal elastic moduli. In reference 8, an analytical solution for an unbalanced, unsymmetrically laminated circular cylindrical shell that is subjected to internal pressure is presented that is based on a variant of the Love-Kirchhoff shell theory, which uses an expression for the change in surface twist that was given by Timoshenko. Numerical results that demonstrate the coupling effects of the shell anisotropies are also presented for a two-ply shell.

The bending boundary layers of an unbalanced, unsymmetrically laminated circular cylindrical shell that is subjected to axial compression, torsion, or thermal loading are investigated in reference 9. Results are also presented that demonstrate the coupling effects of the shell anisotropies. In addition, results are presented for two more conventional unsymmetric laminates and a typical quasi-isotropic laminate. In references 10 and 11, bending boundary layers are also examined for balanced, symmetrically laminated and balanced, unsymmetrically laminated cylindrical shells, in the context of nonlinear prebuckling deformations that occur as a result of compression and thermal loads. In particular, the effects of laminate stacking sequence on the extent and character of the bending boundary layers are presented for two groups of three similar laminates. Two of the laminates are unsymmetric. In reference 12, a linear analysis is presented that focuses mainly on balanced, symmetrically laminated cylinders, and an expression is given for the length of the bending boundary layers near the cylinder ends that is based on the Love-Kirchhoff shell equations.

Most recently, Goldenveizer's static-geometric duality principle (ref. 15) has been used in reference 13 to reduce the Sanders-Koiter equations (refs. 16 and 17) for fully anisotropic, right-circular cylindrical shells to two coupled, fourth-order equations that use a stress and a curvature function as the unknown, primary field variables. The reduction is done by adding certain negligibly small terms to the stress-strain relations, which are intrinsically in error because they must be established experimentally. The approach demonstrates how the static-geometric duality principle can be used to reduce greatly the amount of algebra needed to obtain results. Eigenfunction solutions are also presented for specially orthotropic cylinders that are in agreement with corresponding results presented in reference 6. Moreover, asymptotic formulas that can be used to determine axisymmetric bending boundary-layer attenuation lengths and the decay of other unsymmetric, self-equilibrated edge loads are given.

With the exception of reference 13, explicit expressions for estimating the size of axisymmetric bending boundary layers in fully anisotropic, right-circular cylinders are not found in the literature. Moreover, there appear to be even fewer results for laminated-composite shells made of contemporary material systems and essentially no substantial parametric studies. The present paper focuses on developing meaningful estimates of attenuation lengths of bending boundary layers in balanced and unbalanced, symmetrically and unsymmetrically laminated circular cylinders. The analysis is based on the linear Sanders-Koiter shell equations and contains the Love-Kirchhoff shell equations (ref. 1) and Donnell's equations (ref. 1) as special cases, and is somewhat similar to the analyses presented by Reuter (ref. 4) and Chaudhuri, Balaraman, and Kunukkasseril (ref. 8). With these equations, explicit expressions are obtained and nondimensional parameters are presented that characterize the effects of cylinder geometry and laminate construction on the size of a bending boundary layer in a very general manner. In particular, generic design curves are presented that use the nondimensional parameters to

show the effects of laminate orthotropy and anisotropy on the attenuation length in a concise and encompassing manner. In addition, values of these parameters are presented for a very wide range of orthotropic and anisotropic laminate constructions. Also, differences in the results that were obtained in the present study by using the Sanders-Koiter shell equations, the Love-Kirchhoff shell equations, and Donnell's equations are discussed. Key details of the analysis presented are elaborated upon in appendixes A–C. An example problem is included in appendix D that demonstrates how to perform the calculations that were used to generate the results of the present study.

Analysis

The ordinary differential equation that governs the axisymmetric bending behavior of a right-circular cylinder that is subjected to edge loads or displacements and surface tractions is obtained by first specializing the linear Sanders-Koiter shell equations that are given in appendix A for axial symmetry. For the equations presented herein, x and θ denote the axial and circumferential coordinates of a right-circular cylinder, respectively, and the specialization to axial symmetry is obtained by eliminating all terms in the equations that are differentiated with respect to the circumferential coordinate θ. The resulting set of equations for axisymmetric behavior is given in appendix B. The ordinary differential equation that governs the axisymmetric bending behavior of a right-circular cylinder that is subjected to edge loads or displacements and surface tractions is derived in appendix B and is given by

$$\frac{d^4w}{dx^4} + 4S\frac{d^2w}{dx^2} + 4Qw = P(x) \tag{1}$$

where S, Q, and $P(x)$ are defined in appendix B by equations (B55), (B56), and (B57), respectively, and $w(x)$ is the radial deflection that is positive valued when outward. The coefficients of equation (1) depend on the subscripted A, B, and D constitutive terms of classical Love-Kirchhoff-type laminated shell theory (e.g., see ref. 18, pp. 190–202) and the radius of the cylinder middle surface R.

To determine the specific form of the solution to equation (1), it is useful to examine the positive-definiteness conditions on the strain-energy density function. The strain-energy density function for this problem is given by

$$2\mathcal{U} = N_x\varepsilon_x^o + N_\theta\varepsilon_\theta^o + N_{x\theta}\gamma_{x\theta}^o + M_x\kappa_x^o + M_{x\theta}\kappa_{x\theta}^o \tag{2}$$

where N_x, N_θ, and $N_{x\theta}$ are the membrane stress resultants, M_x and $M_{x\theta}$ are the bending stress resultants, ε_x^o, ε_θ^o, and $\gamma_{x\theta}^o$ are the middle-surface membrane strains, and κ_x^o and $\kappa_{x\theta}^o$ are the middle-surface bending strains. By using equations (B22), (B23), and (B28), the strain-energy density function is expressed as

$$2\mathcal{U} = N_x\varepsilon_x^o + N_\theta\varepsilon_\theta^o + \hat{T}\gamma_{x\theta}^o + M_x\kappa_x^o \tag{3}$$

The strain-energy density is expressed in terms of the strains and constitutive terms by using the constitutive equation given by equation (B29); that is,

$$\mathcal{U} = \frac{1}{2}\begin{Bmatrix} \varepsilon_x^o \\ \varepsilon_\theta^o \\ \gamma_{x\theta}^o \\ \kappa_x^o \end{Bmatrix}^T \begin{bmatrix} A_{11} & A_{12} & \bar{A}_{16} & B_{11} \\ A_{12} & A_{22} & \bar{A}_{26} & B_{12} \\ \bar{A}_{16} & \bar{A}_{26} & \bar{A}_{66} & \bar{B}_{16} \\ B_{11} & B_{12} & \bar{B}_{16} & D_{11} \end{bmatrix} \begin{Bmatrix} \varepsilon_x^o \\ \varepsilon_\theta^o \\ \gamma_{x\theta}^o \\ \kappa_x^o \end{Bmatrix} \tag{4}$$

The stiffness terms in equation (4) that have overbars are defined by equations (B31)–(B35) and are functions of the shell wall thickness-to-radius parameter, $\frac{h}{R}$. By enforcing positive definiteness of the strain-energy density function (e.g., see ref. 19), the requirement that the diagonal terms A_{11}, A_{22}, $\bar{A}_{66}$, and D_{11} be positive valued is obtained. Moreover, the following determinants are positive valued:

$$\begin{vmatrix} A_{11} & A_{12} \\ A_{12} & A_{22} \end{vmatrix} = A_{11}A_{22} - A_{12}^2 > 0 \tag{5}$$

$$\begin{vmatrix} A_{11} & A_{12} & \bar{A}_{16} \\ A_{12} & A_{22} & \bar{A}_{26} \\ \bar{A}_{16} & \bar{A}_{26} & \bar{A}_{66} \end{vmatrix} = \left(A_{11}A_{22} - A_{12}^2\right)\bar{A}_{66} - A_{11}\bar{A}_{26}^2 - A_{22}\bar{A}_{16}^2 + 2A_{12}\bar{A}_{16}\bar{A}_{26} > 0 \tag{6}$$

Likewise, positive definiteness of the strain-energy density function also requires that the determinant of the constitutive matrix in equation (4) be positive valued. Moreover, by rearranging the strain-energy density function into the form

$$\mathcal{U} = \frac{1}{2}\begin{Bmatrix} \varepsilon_x^o \\ \gamma_{x\theta}^o \\ \varepsilon_\theta^o \\ \kappa_x^o \end{Bmatrix}^T \begin{bmatrix} A_{11} & \bar{A}_{16} & A_{12} & B_{11} \\ \bar{A}_{16} & \bar{A}_{66} & \bar{A}_{26} & \bar{B}_{16} \\ A_{12} & \bar{A}_{26} & A_{22} & B_{12} \\ B_{11} & \bar{B}_{16} & B_{12} & D_{11} \end{bmatrix} \begin{Bmatrix} \varepsilon_x^o \\ \gamma_{x\theta}^o \\ \varepsilon_\theta^o \\ \kappa_x^o \end{Bmatrix} \tag{7}$$

the following additional positive-definiteness condition is obtained:

$$\begin{vmatrix} A_{11} & \bar{A}_{16} \\ \bar{A}_{16} & \bar{A}_{66} \end{vmatrix} = A_{11}\bar{A}_{66} - \bar{A}_{16}^2 > 0 \tag{8}$$

The homogeneous solution for equation (1) involves the square root of the quantity $Q - S^2$. By using equations (B55) and (B56), this quantity is given by

$$Q - S^2 = \frac{4C_1C_3 - C_2^2}{16C_1^2} \tag{9}$$

Substituting equations (B41)–(B43) into equation (9) and simplifying, the quantity $Q - S^2$ is found to be given by

$$Q - S^2 = \frac{1}{4C_1^2}\begin{vmatrix} A_{11} & A_{12} & \bar{A}_{16} & B_{11} \\ A_{12} & A_{22} & \bar{A}_{26} & B_{12} \\ \bar{A}_{16} & \bar{A}_{26} & \bar{A}_{66} & \bar{B}_{16} \\ B_{11} & B_{12} & \bar{B}_{16} & D_{11} \end{vmatrix} \tag{10}$$

It follows logically that $Q - S^2 > 0$ because the positive-definiteness of the strain-energy density function requires that the determinant in equation (10) be positive valued. Moreover, $Q - S^2 > 0$ implies that Q > 0, and Q > 0 implies that $\frac{C_3}{C_1} > 0$. Equations (6), (8), and (B43) indicate that $C_3 > 0$. Thus, $\frac{C_3}{C_1} > 0$ yields the condition that $C_1 = D_{11}\boldsymbol{e} > 0$ (see eqs. (B49) and (B50)). Because $D_{11} > 0$; $\boldsymbol{e} > 0$. Because Q is always positive, it is convenient to introduce the expression

$$T^2 = Q = \frac{1}{4R^2\bar{a}_{22}D_{11}\boldsymbol{e}} \tag{11}$$

such that $T^2 - S^2 > 0$, and to express equation (1) as

$$\frac{d^4w}{dx^4} + 4S\frac{d^2w}{dx^2} + 4T^2w = P(x) \tag{12}$$

Equation (12) is a linear, fourth-order, nonhomogeneous ordinary differential equation with constant coefficients. The characteristic equation of equation (12) is given by

$$\lambda^4 + 4S\lambda^2 + 4T^2 = 0 \tag{13}$$

By using the knowledge that $T^2 - S^2 > 0$, the roots of the characteristic equation are obtained from the quadratic formula; that is,

$$\left(\lambda^2\right)_{1,2} = 2\left(-S \pm i\sqrt{T^2 - S^2}\right) \tag{14}$$

where $i = \sqrt{-1}$. Solution of this equation for λ yields four roots of equation (13) that are pairs of complex conjugates given by

$$\lambda_{1,2,3,4} = \pm\left(\sqrt{T - S} \pm i\sqrt{T + S}\right) \tag{15}$$

The homogeneous solution of equation (12) can be written as follows:

$$w_H(x) = K_1 e^{-\sqrt{T-S}\,x} \sin\left(\sqrt{T+S}\,x + K_2\right) + K_3 e^{-\sqrt{T-S}\,(L-x)} \sin\left(\sqrt{T+S}\,x + K_4\right) \tag{16a}$$

where $x \in [0,L]$. The symbols K_1, K_2, K_3, and K_4 are real-valued constants that are determined from the boundary conditions given by equations (B18) and (B19). The solution given by equation (16a) represents a damped, oscillatory response that decays from each end of the cylinder. The regions near the edges of the cylinder, where the amplitude of $w_H(x)$ is the largest, are called the bending boundary layers. All response quantities that exhibit bending boundary layers involve derivatives of equation (16a) and can be expressed in the general form

$$F(x) = F_1 e^{-\sqrt{T-S}\,x} \sin\left(\sqrt{T+S}\,x + F_2\right) + F_3 e^{-\sqrt{T-S}\,(L-x)} \sin\left(\sqrt{T+S}\,x + F_4\right) \tag{16b}$$

where F_1 through F_4 are constants.

When the length of the bending boundary layers is less than half the cylinder length, which is typical, equations (16) can be partitioned into one part that applies to the edge $x = 0$ and the other that applies to the edge $x = L$. The response quantities for the region near $x = 0$ are obtained by setting $F_3 = 0$ in equation (16b). Similarly, the response quantities for the region near $x = L$ are obtained by setting $F_1 = 0$ in equation (16b).

Formulas for Attenuation Length

Formulas for the attenuation or decay length of the bending boundary layers are obtained by first noting that the response quantities for the region near $x = 0$ are bounded by the two functions $\pm F_1 e^{-\sqrt{T-S}\,x}$ and that the response quantities for the region near $x = L$ are bounded by the two functions $\pm F_3 e^{-\sqrt{T-S}\,(L-x)}$. Let d denote the length for which the solution attenuates or decays to a value of ε times the amplitude F_1 or F_3. A reasonable estimate of the attenuation length or decay length d is obtained by replacing x and $(L - x)$ with d in the exponential terms of equation (16b) and by noting that the amplitude of $F(x)$ is attenuated by the exponential terms. Thus, the attenuation length or decay length is given by $e^{-\sqrt{T-S}\,d} = \varepsilon$, which yields

$$d = -\ln \varepsilon (T - S)^{-1/2} < \frac{L}{2} \tag{17}$$

By using equations (B55) and (11), equation (17) is expressed as

$$\frac{d}{\sqrt{Rh}} = \frac{d^o}{\sqrt{Rh}} \mathcal{A} \tag{18}$$

where d^o is the attenuation length, in which anisotropy is neglected ($\mathcal{A} = 1$), that is, given in nondimensional form by

$$\frac{d^o}{\sqrt{Rh}} = -\frac{\ln \varepsilon}{\sqrt[4]{3}} \mathcal{O} \tag{19}$$

The symbol h is the shell wall thickness, and $\mathcal{O}$ and $\mathcal{A}$ are nondimensional orthotropy and anisotropy parameters or factors, respectively, that are given by

$$\mathcal{O} = \left[\frac{12A_{11}D_{11}}{(A_{11}A_{22} - A_{12}^2)h^2}\right]^{1/4} \tag{20a}$$

$$\mathcal{A} = \left(\frac{A_{11}A_{22} - A_{12}^2}{A_{11}} \bar{a}_{22} \mathcal{e}\right)^{1/4} \left(1 - \frac{\bar{b}_{21}}{\sqrt{\bar{a}_{22}D_{11}\mathcal{e}}}\right)^{-1/2} \tag{20b}$$

where the symbols in these equations are defined in appendix B.

Other useful forms of equation (20a) are obtained by introducing an effective membrane Poisson's ratio $\nu_m = \frac{A_{12}}{\sqrt{A_{11}A_{22}}}$, which is the geometric mean of the two Poisson effects associated with the inplane principal direction of a homogenized orthotropic material. By using this effective membrane Poisson's ratio, equation (20a) is expressed as

$$\mathcal{O} = \left[\frac{12D_{11}}{A_{22}h^2(1 - \nu_m^2)}\right]^{1/4} \tag{21}$$

For a single layer of homogeneous, specially orthotropic material, $\nu_m = \sqrt{\nu_{12}\nu_{21}}$, $\mathcal{A} = 1$, and

$$\mathcal{O} = \left[\frac{E_1}{E_2(1 - \nu_{12}\nu_{21})}\right]^{1/4} \tag{22}$$

which, when substituted into equation (19), yields results identical to the results presented by Kraus (ref. 1), where the decay tolerance is given by $\varepsilon = e^{-\pi}$. Likewise, for a single layer of isotropic material with an arbitrary thickness, $\nu_m = \nu$, $\mathcal{A} = 1$, and

$$\mathcal{O} = \frac{1}{\sqrt[4]{(1-\nu^2)}} \tag{23}$$

For values of $0.2 \le \nu \le 0.33$, $\mathcal{O}$ varies by less than 2 percent. A 90-percent-decay length ($\varepsilon = 0.1$) that is a good approximation to the behavior of homogeneous, metallic shells is given by $\frac{d^o}{R} = 1.79\sqrt{\frac{h}{R}}$. Applying this formula, for example, to the Space Shuttle solid rocket booster described in references 20 and 21 (R = 72 in., h = 0.5 in.) gives d^o = 0.15R = 10.8 in.

It is interesting to note that the differences between the attenuation lengths that are based on the Sanders-Koiter, the Love-Kirchhoff, and Donnell's equations appear in the coefficient $\mathcal{e}$ and in the symbols with overbars in equation (20b) for the anisotropy factor $\mathcal{A}$ (see eqs. (B22), (B31)–(B35), and (B45)–(B49)). For these equations, the Sanders-Koiter theory is given by $\mu = \frac{3}{2}$ and the Love-Kirchhoff theory is given by $\mu = 1$. Donnell's equations are given by $\mu = 0$. For isotropic and specially orthotropic cylinders, $\mathcal{A} = 1$ and the three sets of shell equations yield identical results. Similarly, for antisymmetric cross-ply cylinders ($A_{16} = A_{26} = D_{16} = D_{26} = B_{16} = B_{26} = B_{12} = B_{66} = 0$)

$$\mathcal{A} = \left(1 - \frac{B_{11}^2}{A_{11}D_{11}}\right)^{1/4} \left[1 - \frac{A_{12}B_{11}}{\sqrt{(A_{11}A_{22} - A_{12}^2)(A_{11}D_{11} - B_{11}^2)}}\right]^{-1/2} \tag{24}$$

and the three shell theories yield identical results.

Simplified Formulas for $\mathcal{A}$

For balanced, symmetrically laminated cylinders, the only anisotropic constitutive terms are D_{16} and D_{26}, and the anisotropy factor is given by $\mathcal{A} = \sqrt[4]{\mathcal{e}}$ where

$$\mathcal{e} = 1 - \frac{\mu^2 D_{16}^2}{A_{66}D_{11}h^2}\left[\frac{\left(\frac{h}{R}\right)^2}{1 + \mu^2\left(\frac{h}{R}\right)^2 \frac{D_{66}}{A_{66}h^2}}\right] \tag{25}$$

For thin-shell theories, such as the Sanders-Koiter theory and the Love-Kirchhoff theory, $\frac{h}{R} \le \frac{1}{20}$. This result suggests that a useful approximation to equation (25) and the anisotropy factor can be obtained from a power series expansion for small values of $\frac{h}{R}$. This process yields

$$\mathcal{A} \approx 1 - \frac{\mu^2}{4}\left(\frac{h}{R}\right)^2 \frac{D_{16}^2}{A_{66}D_{11}h^2} \tag{26}$$

In this expression, $0 \le \mu \le \frac{3}{2}$ and $0 \le \frac{D_{16}^2}{A_{66}D_{11}h^2} < 1$. Thus, the approximate formula for $\mathcal{A}$ indicates that for most practical applications of thin-shell theory, the differences between the three different shell theories considered herein and the effect of the flexural anisotropy of a general symmetrically laminated cylinder are negligible.

A simplified formula for the anisotropy factor can be derived for the general expression for $\mathcal{A}$ that is given by equation (20b). For this case, the following power series expansions for small values of $\frac{h}{R}$ are used:

$$\boldsymbol{e} = \boldsymbol{e}_0 + \boldsymbol{e}_1\left(\frac{h}{R}\right) + \boldsymbol{e}_2\left(\frac{h}{R}\right)^2 + \cdots \tag{27}$$

$$\bar{a}_{12} = a_{12} + a_{112}\left(\frac{h}{R}\right) + a_{212}\left(\frac{h}{R}\right)^2 + \cdots \tag{28}$$

$$\bar{a}_{22} = a_{22} + a_{122}\left(\frac{h}{R}\right) + a_{222}\left(\frac{h}{R}\right)^2 + \cdots \tag{29}$$

$$\bar{a}_{26} = a_{26} + a_{126}\left(\frac{h}{R}\right) + a_{226}\left(\frac{h}{R}\right)^2 + \cdots \tag{30}$$

$$\bar{b}_{21} = b_{21} + b_{121}\left(\frac{h}{R}\right) + b_{221}\left(\frac{h}{R}\right)^2 + \cdots \tag{31}$$

Substituting equations (27)–(31) into equation (20b) and expanding the resulting expression in a similar manner yields

$$\mathcal{A} = \mathcal{A}_0 + \mathcal{A}_1\left(\frac{h}{R}\right) + \mathcal{A}_2\left(\frac{h}{R}\right)^2 + \cdots \tag{32}$$

The coefficient $\mathcal{A}_2$ is a very complicated expression, and as a result, the following first-order approximation of $\mathcal{A}$ is used herein; that is,

$$\mathcal{A} \approx \mathcal{A}_0 \left[1 + \mu \mathcal{C}_1 \left(\frac{h}{R} \right) \right] \tag{33}$$

where $\mathcal{A}_0$ is the value of equation (20b) with $\mu = 0$, which is the anisotropy factor that corresponds to the use of Donnell's equations. The expression for $\mathcal{A}_0$ is given by

$$\mathcal{A}_0 = \left(\frac{A_{11}A_{22} - A_{12}^2}{A_{11}} a_{22} \mathcal{e}_0 \right)^{1/4} \left(1 - \frac{b_{21}}{\sqrt{a_{22} D_{11} \mathcal{e}_0}} \right)^{-1/2} \tag{34}$$

In this expression, a_{22} and b_{21} are obtained from equations (B45)–(B48) by setting $\mu = 0$ in equations (B31)–(B35). The expression for $\mathcal{e}_0$ is obtained from equation (B49) in a similar manner. The term $\mathcal{C}_1$ in equation (33) represents a first-order correction to the results that correspond to Donnell's equations and is given by

$$\mathcal{C}_1 = \frac{\sqrt{a_{22} D_{11} \mathcal{e}_0} \left(a_{22} \mathcal{e}_1 + a_{122} \mathcal{e}_0 \right) + 2a_{22} \left(b_{121} \mathcal{e}_0 - b_{21} \mathcal{e}_1 \right) - 2a_{122} b_{21} \mathcal{e}_0}{4a_{22} \mathcal{e}_0 \left(\sqrt{a_{22} D_{11} \mathcal{e}_0} - b_{21} \right)} \tag{35}$$

where the terms that appear in equation (35) are given in appendix C. In addition, further simplifications to $\mathcal{A}_0$ and $\mathcal{C}_1$ are also presented in appendix C for unbalanced and balanced symmetric laminates and for balanced, unsymmetric laminates that include the subclasses of general antisymmetric laminates, antisymmetric cross-ply laminates, and antisymmetric angle-ply laminates. The relative size of $\mathcal{C}_1$ and its contribution to equation (33) are examined parametrically in the subsequent section of the present study.

Results and Discussion

Equations (18) and (19) form the basis for the parametric study presented herein. In particular, the two equations isolate the contributions of shell orthotropy and shell anisotropy to the bending boundary-layer decay length with nondimensional parameters and imply the generic design-chart representations that are illustrated in figures 1 and 2. In figure 1, generic results are presented that show the nondimensional, 90-percent-decay length given by $\left. \frac{d}{\sqrt{Rh}} \right|_{\varepsilon = 0.1}$, as a function of the orthotropy parameter $\mathcal{O}$, for selected values of the anisotropy parameter $\mathcal{A}$. A 90-percent-decay length was selected herein to yield an accuracy that is approximately to within the accuracy of the experimentally determined material properties, but other values could be used.

In a manner similar to figure 1, figure 2 shows the nondimensional, 90-percent-decay length, as a function of the anisotropy parameter $\mathcal{A}$, for selected values of the orthotropy parameter $\mathcal{O}$. Results that correspond to balanced, symmetrically laminated cylinders are given by a value of $\mathcal{A} = 1$, and results

that correspond to an isotropic shell wall are indicated in the figures by the filled circle with an ordinate value of 1.79. Overall, these two figures represent results that are applicable to a vast range of laminate constructions and provide a common basis for comparison of regular and hybrid laminates made of different material systems and laminate stacking sequences. In general, the figures show increases in the nondimensional 90-percent-decay length, with increases in either the orthotropy parameter $\mathcal{O}$ or the anisotropy parameter $\mathcal{A}$. In addition, the results in figures 1 and 2 clearly indicate the effect of neglecting shell-wall anisotropy on the attenuation of a bending boundary layer.

The actual value of the nondimensional, 90-percent-decay length depends on the particular values of the orthotropy and anisotropy parameters of a given laminate. Thus, additional results are presented subsequently that show how the orthotropy parameter $\mathcal{O}$ and the anisotropy parameter $\mathcal{A}$ vary with laminate construction. In particular, values of $\mathcal{O}$ and $\mathcal{A}$ are presented first for balanced and unbalanced symmetrically laminated cylinders. Then, values are presented for balanced and unbalanced unsymmetrically laminated cylinders. Nine different contemporary material systems were used to generate these results. These material systems include boron-aluminum, S-glass-epoxy, a typical boron-epoxy, AS4/3501-6 graphite-epoxy, AS4/3502 graphite-epoxy, IM7/5260 graphite-bismaleimide, Kevlar 49-epoxy, IM7/PETI-5 graphite-epoxy, and P-100/3502 pitch-epoxy materials. The mechanical properties of these material systems are presented in table 1; the nominal ply thickness that was used is 0.005 in. An example problem in appendix D demonstrates how to perform the calculations that were used to generate the results that are presented subsequently.

Balanced, Symmetrically Laminated Cylinders

Symmetrically laminated shell walls are characterized mathematically by values of zero for the subscripted B terms that appear in the constitutive equation (A15). In addition, balanced, symmetrically laminated shell walls do not exhibit coupling between extension and shear, which is characterized by $A_{16} = A_{26} = 0$ in equation (A15). Shell walls of this class are strictly specially orthotropic for many laminates. However, for some wall constructions, balanced, symmetric laminates exhibit anisotropy in the form of coupling between pure bending and twisting of the shell wall. This type of anisotropy is manifested by nonzero values of the D_{16} and D_{26} constitutive terms in equation (A15). However, the discussion of equation (26) that has been given herein indicates that this type of anisotropy is negligible for thin shells and that the differences between results obtained from the Sanders-Koiter, the Love-Kirchhoff, and the Donnell theories are insignificant. Moreover, $\mathcal{A} = 1$ for this class of laminated-composite shell walls, and the attenuation behavior is governed by the nondimensional orthotropy parameter $\mathcal{O}$ that is given by equation (20a). Furthermore, equations (18) and (19) indicate that the attenuation length is a constant multiple of the orthotropy parameter that depends on the attenuation-tolerance parameter ε. For this case, trends that are exhibited by $\mathcal{O}$ are identical to those exhibited by the attenuation length based on any value of ε.

Values of the orthotropy parameter $\mathcal{O}$ are presented in figure 3 and table 2 for single-ply, homogeneous, specially orthotropic and isotropic shell walls, with arbitrary thickness, as a function of the ratio of the principal elastic moduli, E_2/E_1. For these results, the orthotropy parameter is given by equation (22) and is expressed in the following, more convenient form:

$$\mathcal{O} = \left[\frac{E_2}{E_1}\left(1 - \frac{E_2}{E_1}\nu_{12}^2\right)\right]^{-1/4} \tag{36}$$

One curve (shown in fig. 3), which is essentially several coincident curves, corresponds to general results for $0.2 \le \nu_{12} \le 0.35$. In addition, specific results for the nine material systems considered herein and for a typical aluminum and a steel are indicated by the square symbols in the figure. The results in figure 3 indicate that the effects of variations in the major Poisson's ratio on the orthotropy parameter $\mathcal{O}$ are small compared to the effect of variations in the ratio of the principal elastic moduli. Moreover, the results show that $\mathcal{O}$ decreases rapidly as the ratio of the principal elastic moduli increases, particularly for values of E_2/E_1 less than approximately 0.1, which corresponds to most of the contemporary orthotropic materials considered herein. Figure 3 also shows that an isotropic material corresponds to $\mathcal{O} \approx 1$.

Values of the orthotropy parameter $\mathcal{O}$ for the single-ply, homogeneous, specially orthotropic cylinders investigated by Cheng and He (ref. 6) were also obtained. A comparison of the results obtained in the present study, with the corresponding results of reference 6, is presented in table 3 for boron-epoxy, glass-epoxy, and graphite-epoxy materials and for the cylinder radius-to-thickness ratio R/h = 208.311. Moreover, a range of results is shown for reference 6 that corresponds to various simplifications that were used in the equations that govern the response. The actual material properties that were used are given in reference 6. In table 3, the quantity used for comparison is given by

$$\mathcal{R}e(\mu) = \frac{\sqrt[4]{3}}{\mathcal{O}} \sqrt{\frac{R}{h}} \tag{37}$$

which is the real part of the exponent μ that appears in the eigenfunction solution used by Cheng and He (n = 0 in eq. (25) of ref. 6; see also eq. (47) of ref. 13), which corresponds to the decay or attenuation of the response. The orthotropy parameter shown in equation (37) is defined by equation (36). The results in table 3 show very good agreement (less than 1 percent difference) for all three materials. In addition, the results obtained herein that are shown in table 3 for the boron-epoxy material are also in excellent agreement with the corresponding results presented by McDevitt and Simmonds (ref. 13).

Values of the orthotropy parameter $\mathcal{O}$ are presented in figure 4 and table 4 for multilayered $[(\pm\phi)_m]_s$ laminates made from the nine material systems as a function of the fiber angle ϕ, which is measured from the x-axis toward the θ-axis. The results are independent of the stacking sequence number m and show a wide variation in $\mathcal{O}$ with the material system. The results also show, for the most part, a wide variation in $\mathcal{O}$ with the fiber angle ϕ and a reduction in $\mathcal{O}$ as the fiber angle increases from 0° to 90°. The largest value (2.93) and the smallest value (0.34) of $\mathcal{O}$ are exhibited by the unidirectional laminates made from P-100/3502 pitch-epoxy material and correspond to values of $\left.\frac{d}{\sqrt{Rh}}\right|_{\varepsilon = 0.1}$ equal to 5.13 and 0.59, respectively. Moreover, the greatest variation in $\mathcal{O}$ with the fiber angle (approximately 8.7 times) is exhibited by the laminates made from P-100/3502 pitch-epoxy material. The smallest variation is exhibited by the laminates made from the boron-aluminum material.

Results are presented in figure 5 that show the values of the orthotropy parameter for $[(\pm45/0_2)_m]_s$, $[(0_2/\pm45)_m]_s$, $[(\pm45/90_2)_m]_s$, $[(90_2/\pm45)_m]_s$, $[(\pm45/0/90)_m]_s$, and $[(0/90/\pm45)_m]_s$ laminates made of IM7/5260 graphite-bismaleimide material for values of the stacking sequence number m = 1 to 6. Values of $\mathcal{O}$ range from approximately 1.53 to 0.64. These results show that the curves for the $[(\pm45/0_2)_m]_s$ and $[(0_2/\pm45)_m]_s$ laminates approach $\mathcal{O} \approx 1.41$ as m increases to a value of 6, with the curve for the $[(0_2/\pm45)_m]_s$ laminates converging from above and the other curve converging from below. The higher values of $\mathcal{O}$ for the $[(0_2/\pm45)_m]_s$ laminates are attributed to the higher axial bending stiffness that is obtained by placing the 0° plies at the outer surfaces of the laminates, particularly for the lower values of the stacking sequence number m. Similarly, the results in figure 5 show that the curves

for the $[(\pm 45/90_2)_m]_s$ and $[(90_2/\pm 45)_m]_s$ laminates approach $\mathcal{O} \approx 0.76$ as m increases to a value of 6, with the curve for the $[(\pm 45/90_2)_m]_s$ laminates converging from above and the other curve converging from below. Likewise, the results in figure 5 show that the curves for the $[(\pm 45/0/90)_m]_s$ and $[(0/90/\pm 45)_m]_s$ quasi-isotropic laminates approach $\mathcal{O} \approx 1.03$ as m increases to a value of 6, with the curve for the $[(0/90/\pm 45)_m]_s$ laminates converging from above and the other curve converging from below.

Overall, the results in figure 5 indicate that the $[(\pm 45/0_2)_m]_s$ and $[(0_2/\pm 45)_m]_s$ laminates exhibit higher values of the orthotropy parameter than the $[(\pm 45/0/90)_m]_s$ and $[(0/90/\pm 45)_m]_s$ quasi-isotropic laminates, which exhibit higher values of the orthotropy parameter than the $[(\pm 45/90_2)_m]_s$ and $[(90_2/\pm 45)_m]_s$ laminates. This trend corresponds to a reduction in the value of $\mathcal{O}$ as the axial bending and extensional stiffnesses of the laminates decrease.

Results are presented in figure 6 and table 5 that show the effect of the nine material systems considered herein on the orthotropy parameter for the $[(0_2/\pm 45)_m]_s$ laminates. Values of $\mathcal{O}$ range from approximately 1.67 for P-100/3502 pitch-epoxy material to 1.09 for boron-aluminum material. Most of the materials exhibit values of $\mathcal{O}$ in the range of approximately 1.4 to 1.6. All curves show about the same reduction in $\mathcal{O}$ as the stacking sequence number m increases.

Results similar to those in figure 6 and table 5 are presented in figure 7 and tables 6 and 7 that show the effect of the nine material systems on the orthotropy parameter for the $[(\pm 45/0/90)_m]_s$ and $[(0/90/\pm 45)_m]_s$ quasi-isotropic laminates. These results show a much smaller variation in the orthotropy parameter with material system and stacking sequence number for the quasi-isotropic laminates than for the $[(0_2/\pm 45)_m]_s$ laminates in figure 6. In particular, values of $\mathcal{O}$ for the quasi-isotropic laminates range from approximately 1.15 to 1.0. The largest values of $\mathcal{O}$ in figure 7 are exhibited by the laminates made of the P-100/3502 pitch-epoxy material. Moreover, the results show a larger variation in $\mathcal{O}$ with stacking sequence number for the $[(0/90/\pm 45)_m]_s$ laminates than for the $[(\pm 45/0/90)_m]_s$ laminates.

Unbalanced, Symmetrically Laminated Cylinders

Unbalanced, symmetric laminates exhibit anisotropy in the form of extensional-shear coupling ($A_{16} \neq 0$, $A_{26} \neq 0$) in addition to flexural anisotropy ($D_{16} \neq 0$, $D_{26} \neq 0$). For these laminates, the value of the anisotropy parameter $\mathcal{A}$, given by equations (20b) and (33), is not equal to unity. Simplified expressions for the anisotropy parameter $\mathcal{A}_0$ and the first-order correction factor $\mathcal{C}_1$, defined by equations (33)–(35), are given by equations (C23) and (C24), respectively. Equation (C24) indicates that the value $\mathcal{C}_1$ depends on coupling between the membrane and flexural anisotropies.

Values of the orthotropy parameter $\mathcal{O}$ for $[(+\phi)_{2m}]_s$ symmetric, unidirectional laminates for the nine material systems considered herein are also presented in figure 4 and table 4; that is, the curves presented in figure 4 and the data presented in table 4 for the $[(\pm\phi)_m]_s$ symmetric angle-ply laminates are identical to those for the corresponding $[(+\phi)_{2m}]_s$ symmetric, unidirectional laminates. Thus, the orthotropy behavioral trends for the undirectional laminates are identical to those discussed previously for the symmetric angle-ply laminates and are also independent of the stacking sequence number m.

Results for the anisotropy parameter $\mathcal{A}_0$ and the first-order correction factor $\mathcal{C}_1$ are shown in figure 8 and table 8 and in figure 9, respectively, for the $[(+\phi)_{2m}]_s$ symmetric, unidirectional laminates with the nine material systems considered herein and are independent of the stacking sequence number m. The results in figure 8 and table 8 show a substantial variation in $\mathcal{A}_0$ with fiber orientation and with material system. The results show that $\mathcal{A}_0$ is the most pronounced for values of the fiber angle ϕ between approximately 55° and 80° and that the contribution of the anisotropy to the attenuation behavior is essentially insignificant (<1.05) for values of $\phi < 25°$ and $\phi > 85°$. Moreover, the largest

variation in $\mathcal{A}_0$ with fiber angle is exhibited by the laminates made of the P-100/3502 pitch-epoxy material, and the smallest variation is exhibited by the laminates made of boron-aluminum material. Values of $\mathcal{A}_0$ range from approximately 1.42 for the maximum point on the curve for the P-100/3502 pitch-epoxy material to a value of 1.

The results shown in figure 9 for the first-order correction factor $\mathcal{C}_1$ for the $[(+\phi)_{2m}]_s$ symmetric, unidirectional laminates indicate a substantial relative variation in $\mathcal{C}_1$ with fiber orientation and with material system, but all values of $\mathcal{C}_1$ are less than approximately 0.45. Moreover, $\mathcal{C}_1$ is less than approximately 0.2 for all materials except the P-100/3502 pitch-epoxy material. For the upper bound of thinness of thin-shell theory, given by $\frac{h}{R} = \frac{1}{20}$, the contribution of $\mathcal{C}_1$ to the anisotropy factor defined by equation (33) is practically negligible. Equation (C24) indicates that the insignificance of $\mathcal{C}_1$ means that the coupling of the membrane and flexural anisotropies is negligible for these laminates. The insignificance of $\mathcal{C}_1$ is illustrated and verified in figure 10 for the $[(+\phi)_{2m}]_s$ symmetric, unidirectional laminates made of IM7/5260 graphite-bismaleimide material (black curves) and P-100/3502 pitch-epoxy material (gray curves) for $\frac{h}{R} = \frac{1}{20}$. The finely dashed curves shown in figure 10 correspond to 90-percent-decay lengths for which the anisotropy is neglected. In contrast, the solid curves and the coarsely dashed gray curve include the effect of the membrane anisotropy and are shown for values of μ = 0, 1.0, and 1.5. For these values, results that correspond to the Sanders-Koiter theory and the Love-Kirchhoff theory are given by $\mu = \frac{3}{2}$ and μ = 1.0, respectively. Results that correspond to Donnell's equations are given by μ = 0. The solid curves in figure 10 for μ = 1.0 and 1.5 are based on the exact solution that uses equation (20b) for the anisotropy factor. The corresponding curves that are based on the approximate formula for the anisotropy parameter that is given by equation (33) are identical. The solid curves and the coarsely dashed gray curve indicate that varying μ yields a small effect, which implies that all three shell theories yield essentially the same results and that $\mathcal{A} \approx \mathcal{A}_0$ for the $[(+\phi)_{2m}]_s$ symmetric, unidirectional laminates. Comparing the solid and finely dashed curves in figure 10 also indicates that neglecting the membrane anisotropy underestimates the bending boundary-layer decay length by as much as approximately 31 percent and 21 percent for shell walls made of P-100/3502 pitch-epoxy and IM7/5260 graphite-bismaleimide materials, respectively.

Values of the orthotropy parameter $\mathcal{O}$ for $[(+45_2/0/90)_m]_s$ and $[(0/90/+45_2)_m]_s$ laminates made of the nine material systems considered herein are also presented in figure 7 and in tables 6 and 7, respectively. More specifically, the values of $\mathcal{O}$ for these laminates are identical to the values for the corresponding quasi-isotropic laminates. Results for the anisotropy parameter $\mathcal{A}_0$, defined by equation (34), are shown in figure 11 for $[(+45_2/0/90)_m]_s$ and $[(0/90/+45_2)_m]_s$ laminates made of the nine material systems considered herein. The results in figure 11 are identical for the two laminate families, show no significant variation in $\mathcal{A}_0$ with the stacking sequence number m, and only a slight variation (less than approximately 9 percent) with the material system. Values of $\mathcal{A}_0$ range between approximately 1.1 and 1.0. Corresponding results for the first-order correction factor $\mathcal{C}_1$, defined by equation (35), which are not shown herein, were obtained and indicate that all values of $\mathcal{C}_1$ for the $[(+45_2/0/90)_m]_s$ and $[(0/90/+45_2)_m]_s$ laminates are less than approximately 0.1. These values indicate that the contribution of $\mathcal{C}_1$ to the anisotropy factor defined by equation (33) is practically negligible. Thus, $\mathcal{A} \approx \mathcal{A}_0$ for these laminates. The values of $\mathcal{A}_0$ shown in figure 11 suggest that neglecting the anisotropy would, at most, underestimate the bending boundary-layer decay length by approximately 10 percent. The insignificance of $\mathcal{C}_1$ also means that the coupling of the membrane and flexural anisotropies are unimportant with regard to the primary effect of the individual shell anisotropies that is captured by the parameter $\mathcal{A}_0$.

Balanced, Unsymmetrically Laminated Cylinders

Balanced, unsymmetric laminates may, in general, exhibit anisotropy in the form of coupling between pure bending and twisting ($D_{16} \neq 0$, $D_{26} \neq 0$) and coupling between membrane and bending action, which is manifested by nonzero values for any of the subscripted B-terms in equation (A15). These laminates do not, however, exhibit extensional-shear coupling ($A_{16} = A_{26} = 0$). For the unsymmetric laminates that are discussed subsequently, the first ply in the stacking sequence is the innermost ply of a cylinder. Simplified expressions for the anisotropy parameter $\mathcal{A}_0$ and the first-order correction factor $\mathcal{C}_1$, defined by equations (33)–(35), are given by equations (C27) and (C29), respectively. Equations (C28) and (C29) indicate that the value of $\mathcal{C}_1$ depends on coupling between the flexural anisotropy and the anisotropy caused by unsymmetric lamination.

Results for regular, antisymmetric angle-ply laminates are shown in figures 4 and 12–16, and in tables 4 and 9. In particular, values of the orthotropy parameter $\mathcal{O}$ for $[(\pm\phi)_m]_T$ unsymmetric laminates made of the nine material systems considered herein are also presented in figure 4 and table 4; that is, the orthotropy-parameter curves presented in figure 4 and the data presented in table 4 for the $[(\pm\phi)_m]_s$ symmetric angle-ply laminates are also identical to those for $[(\pm\phi)_m]_T$ unsymmetric laminates. Thus, the orthotropy behavioral trends for the $[(\pm\phi)_m]_T$ unsymmetric laminates are identical to those discussed previously for the corresponding symmetric angle-ply laminates and are also independent of the stacking sequence number m.

Results for the anisotropy parameter $\mathcal{A}_0$ defined by equation (C27) are shown in figure 12 and table 9 for two-ply $[\pm\phi]_T$ unsymmetric laminates made of the nine material systems considered herein. The results in figure 12 show a substantial variation in $\mathcal{A}_0$ with fiber orientation and with material system and also show that $\mathcal{A}_0$ is the most pronounced for values of the fiber angle ϕ between approximately 15° and 60°. Moreover, the largest variation in $\mathcal{A}_0$ with fiber angle is exhibited by the laminates made of the P-100/3502 pitch-epoxy material, and the smallest variation is exhibited by the laminates made of boron-aluminum material. Values of $\mathcal{A}_0$ range from approximately 0.75 for the minimum point on the curve for the P-100/3502 pitch-epoxy material to a value of 1.0. The results in figure 13 show the variation in $\mathcal{A}_0$ with the fiber angle ϕ and the stacking sequence number m for $[(\pm\phi)_m]_T$ unsymmetric laminates made of the P-100/3502 pitch-epoxy material. These results show a rapid decline in the importance of $\mathcal{A}_0$ that is manifested by the curve moving closer to $\mathcal{A}_0 = 1$, as the stacking sequence number increases. For $m = 2$, $0.95 < \mathcal{A}_0 < 1$.

Results for the first-order correction factor $\mathcal{C}_1$ are shown in figure 14 for two-ply $[\pm\phi]_T$ unsymmetric laminates made of the nine material systems considered herein. The results in figure 14 also show a substantial variation in $\mathcal{C}_1$ with fiber orientation and with material system. However, the maximum value of $\mathcal{C}_1 < 0.07$ for all material systems. Results are presented in figure 15 that show the variation in $\mathcal{C}_1$ with the fiber angle ϕ and the stacking sequence number m for $[(\pm\phi)_m]_T$ unsymmetric laminates made of the P-100/3502 pitch-epoxy material. These results show significant reductions in $\mathcal{C}_1$ with an increase in the stacking sequence number.

Overall, the results in figures 14 and 15 indicate that the contribution of $\mathcal{C}_1$ to the anisotropy factor defined by equation (33) is negligible for the upper bound of thinness given by $\frac{h}{R} = \frac{1}{20}$, which means that $\mathcal{A} \approx \mathcal{A}_0$. Thus, the results in figure 12 for the two-ply $[\pm\phi]_T$ unsymmetric laminates indicate that neglecting the shell anisotropy overestimates the bending boundary-layer decay length (because $\mathcal{A}_0 \leq 1$) by as much as approximately 33 and 22 percent for shell walls made of P-100/3502 pitch-epoxy and IM7/5260 graphite-bismaleimide materials, respectively. The insignificance of $\mathcal{C}_1$ is illustrated in figure 16 by the gray and the black curves for the laminates made of P-100/3502 pitch-epoxy

and IM7/5260 graphite-bismaleimide materials, respectively. The solid black and the gray curves are for the upper bound of thin-shell theory that is given by $\frac{h}{R} = \frac{1}{20}$. The finely dashed curves shown in figure 16 correspond to 90-percent-decay lengths for which the anisotropy is neglected. In contrast, the solid curves include the effect of the shell anisotropy and are shown for values of μ = 0, 1.0, and 1.5. The solid curves for μ = 1.0 and 1.5 are based on the exact solution that uses equation (20b). The corresponding curves that are based on the approximate formula for the anisotropy parameter given by equation (33) are identical. The solid curves indicate no significant effect of varying μ, which implies that all three shell theories yield essentially the same results for the $[\pm\phi]_T$ unsymmetric laminates. For $[(\pm\phi)_m]_T$ unsymmetric laminates with m > 1 that are made from any of the nine material systems considered herein, the results in figures 12 through 15 indicate that neglecting the shell-wall anisotropy will have a small effect on the calculation of the bending boundary-layer decay length.

Values of the orthotropy parameter $\mathcal{O}$ and the anisotropy parameter $\mathcal{A}_0$ for $[0_p/90_q]_T$ unsymmetric cross-ply laminates are shown in figure 17 and table 10, and in figure 18 and table 11, respectively, for the nine material systems considered herein and as a function of the percentage of 0° plies. For this class of laminates, equation (20b) simplifies to equation (34); that is, $\mathcal{A} = \mathcal{A}_0$. This simplification means that the anisotropy parameter is independent of μ, which means that all three shell theories considered herein yield identical results.

The results in figure 17 show a large variation in $\mathcal{O}$ with the percentage of 0° plies for most of the material systems. In addition, the results show a large variation in $\mathcal{O}$ with the material system for the laminates that are dominated by 90° plies (less than approximately 10 percent 0° plies) and by 0° plies (more than approximately 80 percent 0° plies). Values of $\mathcal{O}$ vary the most for laminates made of P-100/3502 pitch-epoxy material, with values that range from approximately 0.3 to 2.93. Most of the materials exhibit values of $\mathcal{O}$ in the range of approximately 0.6 to 2.1.

The results in figure 18 also show a large variation in $\mathcal{A}_0$ with the percentage of 0° plies for most of the material systems and a large variation with material system for laminates with < 70 percent 0° plies. Moreover, the results show that $\mathcal{A}_0$ is the most pronounced (most different from a value of 1) for laminates with approximately 15 to 30 percent 0° plies. The largest variation in $\mathcal{A}_0$ with the percentage of 0° plies is exhibited by the laminates made of the P-100/3502 pitch-epoxy material, and the smallest variation is exhibited by the laminates made of boron-aluminum material. Values of $\mathcal{A}_0$ range from approximately 0.57 for the minimum point on the curve for the P-100/3502 pitch-epoxy material to a value of 1. Thus, in some cases neglecting the shell-wall anisotropy overestimates the bending boundary-layer decay length by as much as approximately 75 percent for a shell wall made of P-100/3502 pitch-epoxy material. This result is illustrated in figure 19 by the gray curves. Similar results are presented in figure 19 for $[0_p/90_q]_T$ unsymmetric cross-ply laminates made of IM7/5260 graphite-bismaleimide material (black curves). The solid black and the gray curves include the effect of the shell anisotropy, and the finely dashed curves shown in the figure correspond to 90-percent-decay lengths for which the anisotropy is neglected. The results in figure 19 show that including the effect of anisotropy is particularly important for laminates with less than approximately 70 percent 0° plies and more than approximately 5 percent 0° plies.

Unbalanced, Unsymmetrically Laminated Cylinders

Unbalanced, unsymmetric laminates may, in general, exhibit full anisotropy in the form of coupling between pure bending and twisting ($D_{16} \neq 0$, $D_{26} \neq 0$) and coupling between membrane and bending action, which is manifested by nonzero values for any of the subscripted B-terms in equation (A15), and

extensional-shear coupling ($A_{16} \neq 0$, $A_{26} \neq 0$). The expressions for the anisotropy parameter $\mathcal{A}_0$ and the first-order correction factor $\mathcal{C}_1$ that are given by equations (C2)–(C22) indicate that $\mathcal{A}_0$ exhibits coupling between the membrane anisotropy and the anisotropy that is caused by unsymmetric lamination, and that $\mathcal{C}_1$ exhibits coupling between all three types of anisotropies. One family of laminates that exhibits all these anisotropies is the $[70_p/0_q]_T$ unbalanced, unsymmetric laminates with $p > 0$ and $q \neq 0$.

Values of the orthotropy parameter $\mathcal{O}$ and the anisotropy parameter $\mathcal{A}_0$ for $[70_p/0_q]_T$ unbalanced, unsymmetric laminates are shown in figure 20 and table 12 and in figure 21 and table 13, respectively, for the nine material systems considered herein and as a function of the percentage of 70° plies. The results in figure 20 show a large variation in $\mathcal{O}$, with the percentage of 70° plies for most of the material systems. The results also show a large variation in $\mathcal{O}$ with the material system for the laminates that are dominated by 0° plies (less than approximately 20 percent 70° plies). Values of $\mathcal{O}$ vary the most for laminates made of P-100/3502 pitch-epoxy material, with values that range from approximately 0.5 to 3.0.

The results in figure 21 also show a substantial variation in $\mathcal{A}_0$ with the percentage of 70° plies for most of the material systems and a large variation with material system for laminates with between approximately 45 and 100 percent 70° plies. The largest overall variation in $\mathcal{A}_0$ with the percentage of 70° plies is exhibited by the laminates made of the P-100/3502 pitch-epoxy material, and the smallest variation is exhibited by the laminates made of boron-aluminum material. Values of $\mathcal{A}_0$ range from approximately 1.4 to 0.95, which correspond to the maximum and minimum points, respectively, on the curve for the P-100/3502 pitch-epoxy material.

Results for the first-order correction factor $\mathcal{C}_1$ were also obtained for $[70_p/0_q]_T$ unbalanced, unsymmetric laminates made of the nine material systems considered herein but are not included in the present paper. These results also show a substantial, relative variation in $\mathcal{C}_1$ with the percentage of 70° plies, but overall, the magnitude of $\mathcal{C}_1$ is less than approximately 0.25 for the P-100/3502 pitch-epoxy material and < 0.1 for the other materials. These results indicate that the contribution of $\mathcal{C}_1$ to the anisotropy factor defined by equation (33) is negligible for the upper bound of thin-shell theory that is given by $\frac{h}{R} = \frac{1}{20}$, which means that $\mathcal{A} \approx \mathcal{A}_0$. Thus, the results in figure 21 suggest that, in some cases, neglecting the shell-wall anisotropy may overestimate the bending boundary-layer decay length and, in other cases, may underestimate the decay length. This statement is based on the observation that, for example, when $\mathcal{A}_0 < 1$, including anisotropy reduces the value of the decay length given by equations (18) and (19). The insignificance of $\mathcal{C}_1$ also means that the contribution of the flexural anisotropy to the coupling of the anisotropies is negligible. The insignificance of $\mathcal{C}_1$ is clarified in figure 22 for laminates made of P-100/3502 pitch-epoxy material (gray curves) and of IM7/5260 graphite-bismaleimide material (black curves). The solid black and the gray curves are for the upper bound of thinness given by $\frac{h}{R} = \frac{1}{20}$. The finely dashed curves shown in the figure correspond to 90-percent-decay lengths for which the anisotropy is neglected. In contrast, the solid curves include the effect of the shell anisotropy and are shown for values of $\mu = 0$, 1.0, and 1.5. Moreover, the solid curves for $\mu = 1.0$ and 1.5 are based on the exact solution that uses equation (20b). The corresponding curves that are based on the approximate formula for the anisotropy parameter that is given by equation (33) are identical. The solid curves indicate a negligible effect of varying μ, which verifies that $\mathcal{A} \approx \mathcal{A}_0$ and implies that all three shell theories yield essentially the same results for the $[70_p/0_q]_T$ unbalanced, unsymmetric laminates. In addition, the results show that neglecting the shell-wall anisotropy, for the most part,

underestimates the bending boundary-layer decay length by as much as approximately 16 and 6 percent for shell walls made of P-100/3502 pitch-epoxy and IM7/5260 graphite-bismaleimide materials, respectively, and with approximately 20-percent 70° plies. In addition, the results in figure 22 show that neglecting the shell-wall anisotropy underestimates the bending boundary-layer decay length by as much as approximately 31 and 20 percent for shell walls made of P-100/3502 pitch-epoxy and IM7/5260 graphite-bismaleimide materials, respectively, and with approximately 100-percent 70° plies. There is only a very small range shown in figure 22 where neglecting the shell-wall anisotropy overestimates the bending boundary-layer decay length, and for this region, the effect is negligible.

Concluding Remarks

An analytical study of the attenuation of bending boundary layers in both balanced and unbalanced, symmetrically and unsymmetrically laminated-composite, thin cylindrical shells has been presented for nine contemporary material systems. The analysis is based on the linear Sanders-Koiter shell equations and contains the Love-Kirchhoff shell equations and Donnell's equations as special cases. With this analysis, two nondimensional parameters have been identified that characterize and quantify the effects of laminate orthotropy and laminate anisotropy on the bending boundary-layer decay length in a very general and encompassing manner. The anisotropy parameter includes the effects of anisotropy in the form of coupling between pure bending and twisting that appears in many symmetric laminates to some extent, coupling between extension and shear that is present in unbalanced laminates, and coupling between membrane and bending action that is present in unsymmetric laminates.

A substantial number of structural design technology results for the bending boundary-layer decay length have been presented for a wide range of laminated-composite shell structures that should be useful additions to the structural designer's collection of preliminary design tools. Moreover, the analysis and results should provide additional physical insight into the fundamental behavior of general laminated-composite shell structures and create a common basis for assessing bending boundary-layer attenuation for the vast range of laminate constructions that are possible. Furthermore, the results should be useful for the design of specimens for material characterization tests, for instrumenting structural verification tests, and for defining finite-element meshes. For all the laminate constructions considered in the present study, the results show that the differences between results that were obtained with the Sanders-Koiter shell equations, the Love-Kirchhoff shell equations, and Donnell's equations are negligible. The results also show that the effect of anisotropy in the form of coupling between pure bending and twisting has a negligible effect on the size of the bending boundary-layer decay length of the balanced, symmetrically laminated cylinders considered. Moreover, the results show that the coupling of the membrane and flexural anisotropy and the anisotropy caused by unsymmetric lamination is generally unimportant with regard to the primary effect of the individual shell anisotropies on the bending boundary-layer decay length. The only exception encountered was for unbalanced, unsymmetrically laminated cylinders for which coupling of the membrane anisotropy and the anisotropy caused by unsymmetric lamination is a primary effect, as expected. The results also show that in some cases neglecting the shell anisotropy results in underestimating the bending boundary-layer decay length and in other cases results in an overestimation.

References

1. Kraus, H.: *Thin Elastic Shells—An Introduction to the Theoretical Foundations and the Analysis of Their Static and Dynamic Behavior.* John Wiley & Sons, Inc., 1967, pp. 131–142.

2. Pagano, N. J.; and Whitney, J. M.: Geometric Design of Composite Cylindrical Characterization Specimens. *J. Compos. Mater.*, vol. 4, July 1970, pp. 360–378.

3. Dong, S. B.; Pister, K. S.; and Taylor, R. L.: On the Theory of Laminated Anisotropic Shells and Plates. *J. Aerosp. Sci*., Aug. 1962, pp. 969–975.

4. Reuter, Robert C., Jr.: Analysis of Shells Under Internal Pressure. *J. Compos. Mater.*, vol. 6, Jan. 1972, pp. 94–113.

5. Hennemann, José Carlos Ferraz: Effect of Prebuckling Deformations on Buckling of Laminated Composite Circular Cylindrical Shells. Ph.D. Diss., Southern Methodist Univ., Dallas, Texas, 1975.

6. Cheng, Shun; and He, F. B.: Theory of Orthotropic and Composite Cylindrical Shells, Accurate and Simple Fourth-Order Governing Equations. *J. Appl. Mech.*, vol. 51, Dec. 1984, pp. 736–744.

7. Sayir, M.: Edge Effects in Rotationally Symmetric Composite Shells. *Local Effects in the Analysis of Structures—Studies in Applied Mechanics 12*, Pierre Ladeveze, ed., Elsevier Sci. Publ. Co., Inc., 1985, pp. 161–180.

8. Chaudhuri, Reaz A.; Balaraman, K.; and Kunukkasseril, Vincent X.: Arbitrarily Laminated, Anisotropic Cylindrical Shell Under Internal Pressure. *AIAA J.*, vol. 24, no. 11, Nov. 1986, pp. 1851–1858.

9. Butler, T. A.; and Hyer, M. W.: *The Structural Response of Unsymmetrically Laminated Composite Cylinders*. Tech. Rep. 89-2, Dept. of Mechanical Eng., Univ. of Maryland, Aug. 1989.

10. Hyer, M. W.; and Paraska, P. J.: *Innovative Design of Composite Structures: Axisymmetric Deformations of Unsymmetrically Laminated Cylinders Loaded in Axial Compression*. VPI-E-90-10, Virginia Polytechnic Inst., June 1990.

11. Paraska, Peter J.: *Axisymmetric Deformations and Stresses of Unsymmetrically Laminated Composite Cylinders in Axial Compression With Thermally-Induced Preloading Effects*. CARDEROCKDIV-U-SSM-65-93/03, Carderock Div., Naval Surface Warfare Center, Mar. 1993.

12. Vinson, J. R.: Composite Shell Structures and Their Behavior. *Proceedings of the AIAA/ASME/ASCE/AHS/ASC 38th Structures, Structural Dynamics, and Materials Conference*, Kissimmee, Florida, April 7–10, 1997, pp. 2400–2406.

13. McDevitt, T. J.; and Simmonds, J. G.: Reduction of the Sanders-Koiter Equations for Fully Anisotropic Circular Cylindrical Shells to Two Coupled Equations for a Stress and a Curvature Function. *J. Appl. Mech.*, vol. 66, Sept. 1999, pp. 593–597.

14. Flügge, Wilhelm: *Stresses in Shells.* 2nd ed., Springer-Verlag, 1973.

15. Goldenveizer, A. L.: *Theory of Elastic Thin Shells*. Pergamon Press, 1961.

16. Sanders, J. Lyell, Jr.: *An Improved First-Approximation Theory for Thin Shells.* NASA TR R-24, 1959.

17. Koiter, W. T.: A Consistent First Approximation in the General Theory of Thin Elastic Shells. *Theory of Thin Elastic Shells*, W. J. Koiter, ed., North-Holland Publ. Co., 1960, pp. 12–33.

18. Jones, Robert M.: *Mechanics of Composite Materials.* 2nd ed., Taylor & Francis, Inc., 1999.

19. Zwillinger, Daniel, ed.: *Standard Mathematical Tables and Formulae*. 30th ed., CRC Press, 1996, pp. 133–134.

20. Nemeth, M. P.; and Anderson, M. S.: *Axisymmetric Shell Analysis of the Space Shuttle Solid Rocket Booster Field Joint*. NASA TP-3033, Jan. 1991.

21. Nemeth, M. P.; and Anderson, M. S.: Axisymmetric Shell Analysis of the Space Shuttle Solid Rocket Booster Field Joint. *J. Spacecr. & Rockets*, vol. 27, no. 1, Jan.–Feb. 1990, pp. 85–92.

22. Jaunky, Navin; and Knight, Norman F., Jr.: An Assessment of Shell Theories for Buckling of Circular Cylindrical Laminated Composite Panels Loaded in Axial Compression. *Int. J. Solids & Struct.*, vol. 36, 1999, pp. 3799–3820.

Table 1. Lamina Properties

Lamina property (*a*)	Material systems								
	Boron-Al	S-glass-epoxy	Kevlar 49-epoxy	IM7/5260	AS4/3502	AS4/3501-6	Boron-epoxy	IM7/PETI-5	P-100/3502
E_1, Msi	33	7.5	11.02	22.1	18.5	20.01	29.58	20.35	53.5
E_2, Msi	21	1.7	0.8	1.457	1.64	1.30	2.68	1.16	0.73
ν_{12}	0.23	0.25	0.34	0.258	0.30	0.30	0.23	0.29	0.31
G_{12}, Msi	7.0	0.80	0.33	0.860	0.87	1.03	0.81	0.61	0.76
$\alpha_1 \times 10^6$/°F	3.2	3.5	–2.22	0.0125	0.25	–0.167	3.38	–0.14	–0.64
$\alpha_2 \times 10^6$/°F	11.0	11.0	43.89	14.91	16.2	15.6	16.83	16.85	17.2

[a]Subscripts 1 and 2 denote the longitudinal (fiber) and transverse (matrix) directions of a specially orthotropic lamina, respectively.

Table 2. Orthotropy Parameters for Single-Ply, Homogeneous, Specially Orthotropic Laminates

[See eq. (36)]

E_2/E_1	Orthotropy parameter, $\mathcal{O}$	
	$\nu_{12} = 0.2$	$\nu_{12} = 0.35$
0.01	3.16	3.16
0.02	2.66	2.66
0.04	2.24	2.24
0.06	2.02	2.02
0.08	1.88	1.88
0.1	1.78	1.78
0.15	1.61	1.61
0.2	1.50	1.50
0.3	1.36	1.36
0.4	1.26	1.27
0.5	1.20	1.21
0.6	1.14	1.16
0.7	1.10	1.12
0.8	1.07	1.09
0.9	1.04	1.06
1.0	1.01	1.03

Table 3. Results for Specially Orthotropic Materials

Material systems	E_2/E_1 (*a*)	ν_{12}	$\mathcal{O}$	$\mathcal{R}e(\mu)$, from reference 6 (*b*)	$\mathcal{R}e(\mu)$, from present study (*b*)
Boron-epoxy	0.100	0.30	1.782	2.796–2.805	2.806
Glass-epoxy	0.333	0.25	1.323	3.757–3.779	3.779
Graphite-epoxy	0.250	0.25	2.516	1.984–1.987	1.987

[a]Subscripts 1 and 2 denote the major and minor principal directions, respectively, of the specially orthotropic materials defined in reference 6.

[b]Quantity $\mathcal{R}e(\mu)$ is defined by equation (37).

Table 4. Orthotropy Parameters for $[(\pm\phi)_m]_s$, $[(+\phi)_{2m}]_s$, and $[(\pm\phi)_m]_T$ Laminates

Fiber angle, ϕ	Orthotropy parameter, $\mathcal{O}$								
	IM7/ 5260	Boron-Al	S-glass-epoxy	Kevlar 49-epoxy	AS4/ 3502	AS4/ 3501-6	Boron-epoxy	IM7/ PETI-5	P-100/ 3502
0	1.98	1.13	1.45	1.93	1.84	1.98	1.82	2.05	2.93
5	1.97	1.13	1.45	1.92	1.83	1.97	1.82	2.04	2.90
10	1.94	1.13	1.44	1.91	1.81	1.94	1.81	2.02	2.84
15	1.90	1.12	1.42	1.88	1.77	1.88	1.79	1.98	2.73
20	1.84	1.12	1.39	1.84	1.72	1.80	1.76	1.92	2.58
25	1.76	1.11	1.35	1.78	1.66	1.71	1.72	1.84	2.40
30	1.65	1.10	1.30	1.70	1.57	1.59	1.67	1.74	2.19
35	1.53	1.09	1.24	1.60	1.46	1.46	1.59	1.61	1.97
40	1.39	1.07	1.16	1.46	1.34	1.32	1.48	1.46	1.74
45	1.23	1.05	1.08	1.30	1.20	1.17	1.33	1.29	1.50
50	1.07	1.02	1.00	1.13	1.05	1.03	1.15	1.12	1.26
55	0.92	0.99	0.92	0.96	0.92	0.89	0.97	0.94	1.04
60	0.78	0.97	0.85	0.81	0.80	0.77	0.81	0.79	0.83
65	0.68	0.95	0.79	0.69	0.70	0.68	0.70	0.67	0.65
70	0.60	0.93	0.75	0.61	0.63	0.60	0.62	0.59	0.51
75	0.55	0.92	0.72	0.56	0.59	0.55	0.58	0.53	0.42
80	0.52	0.91	0.71	0.53	0.56	0.52	0.56	0.50	0.37
85	0.51	0.90	0.70	0.52	0.55	0.51	0.55	0.49	0.35
90	0.51	0.90	0.69	0.52	0.55	0.51	0.55	0.49	0.34

Table 5. Orthotropy Parameters for $[(0_2/\pm45)_m]_s$ Laminates

Number of laminate plies, 8m	Orthotropy parameter, $\mathcal{O}$								
	IM7/ 5260	Boron-Al	S-glass-epoxy	Kevlar 49-epoxy	AS4/ 3502	AS4/ 3501-6	Boron-epoxy	IM7/ PETI-5	P-100/ 3502
8	1.53	1.12	1.32	1.54	1.49	1.52	1.52	1.56	1.67
16	1.48	1.10	1.28	1.48	1.44	1.46	1.46	1.50	1.60
24	1.46	1.10	1.27	1.46	1.42	1.44	1.44	1.48	1.58
32	1.45	1.09	1.26	1.45	1.41	1.43	1.43	1.47	1.56
40	1.44	1.09	1.26	1.44	1.40	1.42	1.43	1.46	1.56
48	1.43	1.09	1.25	1.44	1.40	1.42	1.42	1.46	1.55
56	1.43	1.09	1.25	1.44	1.40	1.42	1.42	1.45	1.55
64	1.43	1.09	1.25	1.43	1.40	1.41	1.42	1.45	1.54

Table 6. Orthotropy Parameters for $[(\pm 45/0/90)_m]_s$ and $[(+45_2/0/90)_m]_s$ Laminates

Number of laminate plies, 8m	Orthotropy parameter, $\mathcal{O}$								
	IM7/ 5260	Boron-Al	S-glass-epoxy	Kevlar 49-epoxy	AS4/ 3502	AS4/ 3501-6	Boron-epoxy	IM7/ PETI-5	P-100/ 3502
8	1.00	1.01	1.01	1.00	1.00	1.00	1.00	1.00	1.00
16	1.02	1.02	1.02	1.02	1.02	1.02	1.02	1.02	1.02
24	1.02	1.02	1.02	1.03	1.02	1.02	1.02	1.02	1.03
32	1.02	1.02	1.02	1.03	1.02	1.02	1.03	1.02	1.03
40	1.02	1.02	1.02	1.03	1.02	1.02	1.03	1.03	1.03
48	1.02	1.02	1.02	1.03	1.02	1.02	1.03	1.03	1.03
56	1.02	1.02	1.02	1.03	1.02	1.02	1.03	1.03	1.03
64	1.02	1.02	1.02	1.03	1.02	1.02	1.03	1.03	1.03

Table 7. Orthotropy Parameters for $[(0/90/\pm 45)_m]_s$ and $[(0/90/+45_2)_m]_s$ Laminates

Number of laminate plies, 8m	Orthotropy parameter, $\mathcal{O}$								
	IM7/ 5260	Boron-Al	S-glass-epoxy	Kevlar 49-epoxy	AS4/ 3502	AS4/ 3501-6	Boron-epoxy	IM7/ PETI-5	P-100/ 3502
8	1.13	1.05	1.09	1.14	1.13	1.13	1.14	1.14	1.15
16	1.08	1.04	1.06	1.08	1.07	1.07	1.08	1.08	1.09
24	1.06	1.03	1.04	1.06	1.06	1.06	1.06	1.06	1.07
32	1.05	1.03	1.04	1.06	1.05	1.05	1.05	1.05	1.06
40	1.04	1.03	1.03	1.05	1.04	1.04	1.05	1.05	1.05
48	1.04	1.03	1.03	1.05	1.04	1.04	1.05	1.04	1.05
56	1.04	1.02	1.03	1.04	1.04	1.04	1.04	1.04	1.04
64	1.04	1.02	1.03	1.04	1.04	1.03	1.04	1.04	1.04

Table 8. Anisotropy Parameters for $[(+\phi)_{2m}]_s$ Laminates

Fiber angle, ϕ	Anisotropy parameter, $\mathcal{A}_0$								
	IM7/ 5260	Boron-Al	S-glass-epoxy	Kevlar 49-epoxy	AS4/ 3502	AS4/ 3501-6	Boron-epoxy	IM7/ PETI-5	P-100/ 3502
0	1.00	1.00	1.00	1.00	1.00	1.00	1.00	1.00	1.00
5	1.00	1.00	1.00	1.00	1.00	1.00	1.00	1.00	1.00
10	1.00	1.00	1.00	1.00	1.00	1.00	1.00	1.00	1.01
15	1.00	1.00	1.00	1.00	1.00	1.01	1.01	1.00	1.02
20	1.00	1.00	1.00	1.00	1.00	1.02	1.01	1.00	1.03
25	1.01	1.00	1.00	1.00	1.01	1.03	1.00	1.00	1.05
30	1.02	1.00	1.00	1.00	1.01	1.04	1.00	1.01	1.08
35	1.03	1.00	1.01	1.01	1.02	1.06	1.00	1.03	1.11
40	1.06	1.00	1.02	1.03	1.04	1.08	1.01	1.05	1.14
45	1.09	1.00	1.04	1.06	1.07	1.11	1.05	1.09	1.18
50	1.13	1.01	1.06	1.12	1.11	1.14	1.11	1.13	1.23
55	1.18	1.01	1.08	1.18	1.16	1.17	1.19	1.19	1.28
60	1.22	1.02	1.09	1.25	1.20	1.20	1.27	1.25	1.33
65	1.25	1.02	1.09	1.29	1.22	1.21	1.32	1.29	1.39
70	1.24	1.02	1.08	1.29	1.21	1.19	1.32	1.29	1.42
75	1.20	1.01	1.06	1.24	1.16	1.15	1.27	1.24	1.39
80	1.12	1.01	1.03	1.15	1.10	1.09	1.17	1.15	1.28
85	1.04	1.00	1.01	1.05	1.03	1.03	1.05	1.05	1.10
90	1.00	1.00	1.00	1.00	1.00	1.00	1.00	1.00	1.00

Table 9. Anisotropy Parameters for $[\pm\phi]_T$ Laminates

Fiber angle, ϕ	Anisotropy parameter, $\mathcal{A}_0$								
	IM7/ 5260	Boron-Al	S-glass-epoxy	Kevlar 49-epoxy	AS4/ 3502	AS4/ 3501-6	Boron-epoxy	IM7/ PETI-5	P-100/ 3502
0	1.00	1.00	1.00	1.00	1.00	1.00	1.00	1.00	1.00
5	0.97	1.00	0.99	0.97	0.98	0.98	0.96	0.97	0.93
10	0.92	1.00	0.98	0.91	0.94	0.94	0.90	0.90	0.85
15	0.88	0.99	0.96	0.86	0.90	0.90	0.86	0.86	0.80
20	0.85	0.99	0.94	0.83	0.87	0.87	0.83	0.83	0.77
25	0.83	0.99	0.93	0.82	0.85	0.85	0.82	0.81	0.76
30	0.82	0.99	0.92	0.81	0.84	0.84	0.82	0.81	0.75
35	0.82	0.99	0.92	0.82	0.84	0.84	0.82	0.81	0.75
40	0.83	0.99	0.93	0.82	0.85	0.84	0.83	0.81	0.75
45	0.84	0.99	0.94	0.84	0.86	0.85	0.85	0.82	0.76
50	0.86	1.00	0.95	0.86	0.88	0.86	0.87	0.84	0.77
55	0.88	1.00	0.96	0.89	0.90	0.88	0.90	0.87	0.78
60	0.91	1.00	0.98	0.92	0.93	0.91	0.94	0.90	0.80
65	0.94	1.00	0.99	0.95	0.96	0.93	0.97	0.93	0.84
70	0.97	1.00	0.99	0.97	0.98	0.96	0.99	0.97	0.89
75	0.99	1.00	1.00	0.99	0.99	0.98	1.00	0.99	0.94
80	1.00	1.00	1.00	1.00	1.00	0.99	1.00	1.00	0.98
85	1.00	1.00	1.00	1.00	1.00	1.00	1.00	1.00	1.00
90	1.00	1.00	1.00	1.00	1.00	1.00	1.00	1.00	1.00

Table 10. Orthotropy Parameters for $[0_p/90_q]_T$ Laminates

$\frac{p}{p+q} \times 100\%$	Orthotropy parameter, $\mathcal{O}$								
	IM7/ 5260	Boron-Al	S-glass-epoxy	Kevlar 49-epoxy	AS4/ 3502	AS4/ 3501-6	Boron-epoxy	IM7/ PETI-5	P-100/ 3502
0	0.51	0.90	0.69	0.52	0.55	0.51	0.55	0.49	0.34
5	0.67	0.92	0.77	0.68	0.69	0.67	0.69	0.66	0.63
10	0.76	0.94	0.82	0.76	0.77	0.76	0.77	0.75	0.73
15	0.81	0.95	0.86	0.81	0.82	0.81	0.82	0.81	0.79
20	0.85	0.97	0.89	0.86	0.86	0.85	0.86	0.85	0.84
25	0.89	0.98	0.92	0.89	0.89	0.89	0.89	0.89	0.88
30	0.92	0.98	0.94	0.92	0.92	0.91	0.92	0.91	0.91
35	0.94	0.99	0.96	0.94	0.94	0.94	0.94	0.94	0.93
40	0.96	1.00	0.97	0.96	0.96	0.96	0.96	0.96	0.96
45	0.98	1.00	0.99	0.98	0.98	0.98	0.98	0.98	0.98
50	1.00	1.01	1.00	1.00	1.00	1.00	1.00	1.00	1.00
55	1.02	1.01	1.02	1.02	1.02	1.02	1.02	1.02	1.03
60	1.05	1.02	1.04	1.05	1.05	1.05	1.05	1.05	1.06
65	1.09	1.03	1.06	1.08	1.08	1.09	1.08	1.09	1.10
70	1.13	1.04	1.09	1.13	1.12	1.13	1.12	1.13	1.15
75	1.19	1.05	1.12	1.18	1.17	1.19	1.17	1.19	1.22
80	1.26	1.06	1.17	1.25	1.24	1.26	1.24	1.27	1.31
85	1.35	1.07	1.22	1.35	1.33	1.36	1.33	1.37	1.43
90	1.48	1.09	1.28	1.47	1.44	1.49	1.44	1.50	1.61
95	1.67	1.11	1.36	1.65	1.60	1.67	1.59	1.70	1.93
100	1.98	1.13	1.45	1.93	1.84	1.98	1.82	2.05	2.93

Table 11. Anisotropy Parameters for $[0_p/90_q]_T$ Laminates

$\frac{p}{p+q} \times 100\%$	Anisotropy parameter, $\mathcal{A}_0$								
	IM7/ 5260	Boron-Al	S-glass-epoxy	Kevlar 49-epoxy	AS4/ 3502	AS4/ 3501-6	Boron-epoxy	IM7/ PETI-5	P-100/ 3502
0	1.00	1.00	1.00	1.00	1.00	1.00	1.00	1.00	1.00
5	0.91	1.00	0.98	0.91	0.93	0.91	0.94	0.90	0.72
10	0.84	0.99	0.95	0.85	0.87	0.84	0.88	0.82	0.64
15	0.80	0.99	0.93	0.81	0.83	0.80	0.84	0.78	0.59
20	0.77	0.98	0.91	0.78	0.81	0.77	0.81	0.75	0.57
25	0.75	0.98	0.90	0.76	0.79	0.75	0.80	0.73	0.57
30	0.74	0.98	0.89	0.75	0.78	0.74	0.79	0.73	0.59
35	0.75	0.98	0.88	0.75	0.78	0.74	0.78	0.73	0.61
40	0.75	0.97	0.88	0.76	0.78	0.75	0.79	0.74	0.65
45	0.77	0.97	0.88	0.77	0.79	0.77	0.80	0.76	0.69
50	0.79	0.97	0.89	0.79	0.81	0.79	0.82	0.78	0.73
55	0.82	0.97	0.90	0.82	0.83	0.82	0.84	0.81	0.77
60	0.85	0.98	0.91	0.85	0.86	0.85	0.86	0.84	0.82
65	0.88	0.98	0.92	0.88	0.89	0.88	0.89	0.88	0.86
70	0.91	0.98	0.94	0.91	0.91	0.91	0.92	0.91	0.90
75	0.94	0.98	0.95	0.93	0.94	0.94	0.94	0.94	0.93
80	0.96	0.99	0.97	0.96	0.96	0.96	0.96	0.96	0.96
85	0.98	0.99	0.98	0.97	0.98	0.98	0.98	0.98	0.98
90	0.99	0.99	0.99	0.99	0.99	0.99	0.99	0.99	0.99
95	1.00	1.00	1.00	1.00	1.00	1.00	1.00	1.00	1.00
100	1.00	1.00	1.00	1.00	1.00	1.00	1.00	1.00	1.00

Table 12. Orthotropy Parameters for $[70_p/0_q]_T$ Laminates

$\frac{p}{p+q} \times 100\%$	Orthotropy parameter, $\mathcal{O}$								
	IM7/ 5260	Boron-Al	S-glass-epoxy	Kevlar 49-epoxy	AS4/ 3502	AS4/ 3501-6	Boron-epoxy	IM7/ PETI-5	P-100/ 3502
0	1.98	1.13	1.45	1.93	1.84	1.98	1.82	2.05	2.93
5	1.71	1.11	1.37	1.69	1.63	1.71	1.63	1.75	2.02
10	1.54	1.09	1.30	1.52	1.49	1.54	1.49	1.56	1.70
15	1.41	1.08	1.24	1.41	1.38	1.41	1.38	1.43	1.52
20	1.32	1.07	1.20	1.31	1.30	1.32	1.30	1.33	1.39
25	1.25	1.05	1.16	1.24	1.23	1.25	1.23	1.25	1.29
30	1.19	1.05	1.13	1.19	1.18	1.19	1.18	1.20	1.22
35	1.15	1.04	1.10	1.15	1.14	1.15	1.14	1.15	1.17
40	1.11	1.03	1.08	1.11	1.11	1.11	1.11	1.12	1.13
45	1.09	1.03	1.06	1.09	1.08	1.09	1.08	1.09	1.10
50	1.06	1.03	1.05	1.06	1.06	1.06	1.06	1.06	1.07
55	1.04	1.02	1.03	1.04	1.04	1.04	1.04	1.04	1.05
60	1.02	1.02	1.02	1.02	1.02	1.02	1.02	1.02	1.02
65	1.00	1.01	1.00	1.00	1.00	1.00	1.00	1.00	1.00
70	0.98	1.01	0.99	0.98	0.98	0.98	0.98	0.98	0.97
75	0.95	1.00	0.97	0.95	0.95	0.95	0.96	0.95	0.95
80	0.92	0.99	0.94	0.92	0.92	0.92	0.92	0.92	0.91
85	0.88	0.98	0.91	0.88	0.88	0.88	0.89	0.88	0.86
90	0.82	0.97	0.88	0.83	0.83	0.82	0.83	0.82	0.80
95	0.74	0.95	0.83	0.75	0.76	0.74	0.76	0.74	0.71
100	0.60	0.93	0.75	0.61	0.63	0.60	0.62	0.59	0.51

Table 13. Anisotropy Parameters for $[70_p/0_q]_T$ Laminates

$\frac{p}{p+q} \times 100\%$	Anisotropy parameter, $\mathcal{A}_0$								
	IM7/ 5260	Boron-Al	S-glass-epoxy	Kevlar 49-epoxy	AS4/ 3502	AS4/ 3501-6	Boron-epoxy	IM7/ PETI-5	P-100/ 3502
0	1.00	1.00	1.00	1.00	1.00	1.00	1.00	1.00	1.00
5	1.02	1.01	1.01	1.02	1.02	1.02	1.02	1.03	1.07
10	1.04	1.01	1.02	1.05	1.04	1.04	1.05	1.05	1.13
15	1.06	1.02	1.02	1.07	1.05	1.05	1.07	1.08	1.17
20	1.07	1.02	1.03	1.09	1.06	1.05	1.09	1.09	1.19
25	1.07	1.02	1.03	1.10	1.06	1.05	1.10	1.10	1.20
30	1.07	1.03	1.03	1.10	1.06	1.04	1.11	1.09	1.20
35	1.06	1.03	1.03	1.10	1.05	1.03	1.11	1.09	1.18
40	1.05	1.03	1.03	1.09	1.04	1.01	1.12	1.08	1.16
45	1.03	1.04	1.03	1.09	1.04	1.00	1.12	1.06	1.12
50	1.02	1.04	1.03	1.08	1.03	0.98	1.12	1.05	1.08
55	1.01	1.04	1.03	1.08	1.02	0.97	1.13	1.04	1.05
60	1.01	1.04	1.03	1.08	1.02	0.96	1.14	1.04	1.01
65	1.01	1.04	1.04	1.09	1.03	0.96	1.15	1.04	0.98
70	1.02	1.04	1.05	1.11	1.04	0.97	1.18	1.05	0.96
75	1.04	1.04	1.06	1.13	1.06	0.98	1.20	1.07	0.96
80	1.07	1.04	1.07	1.16	1.09	1.00	1.24	1.10	0.97
85	1.11	1.04	1.08	1.20	1.12	1.04	1.28	1.15	1.01
90	1.16	1.03	1.09	1.25	1.16	1.09	1.32	1.20	1.08
95	1.22	1.03	1.10	1.31	1.20	1.15	1.36	1.27	1.21
100	1.24	1.02	1.08	1.29	1.21	1.19	1.32	1.29	1.42

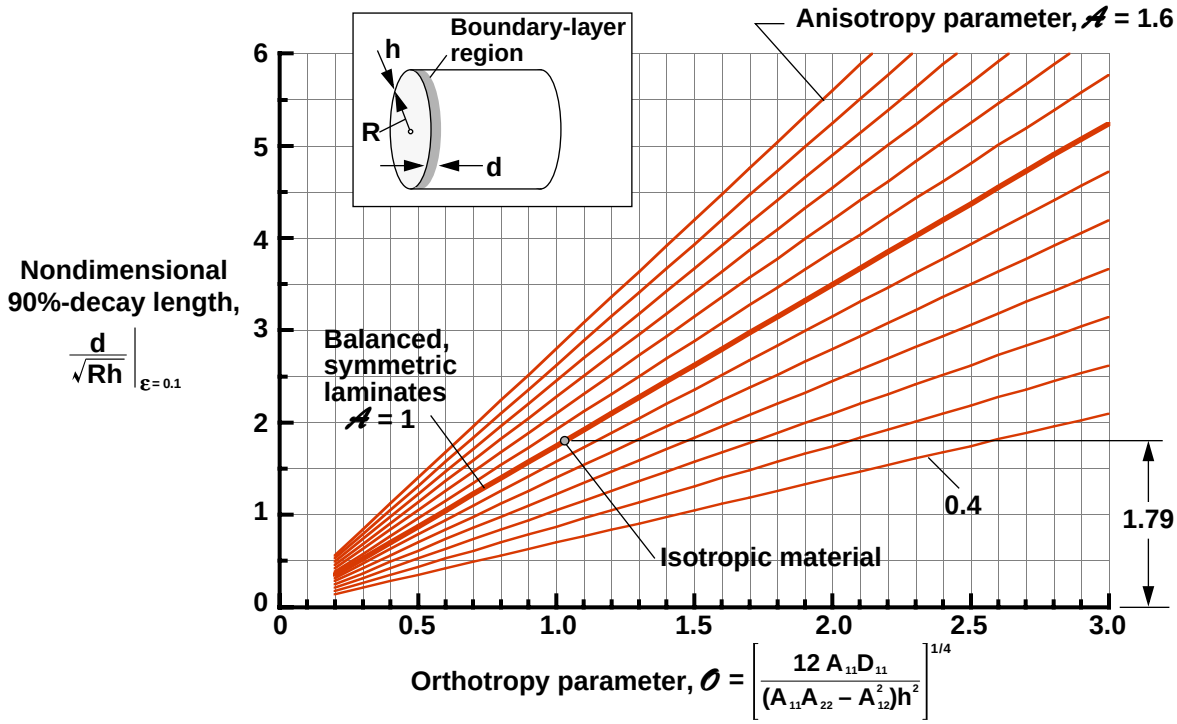

Figure 1. Nondimensional 90-percent-decay length for symmetrically and unsymmetrically laminated cylinders, as a function of laminate orthotropy.

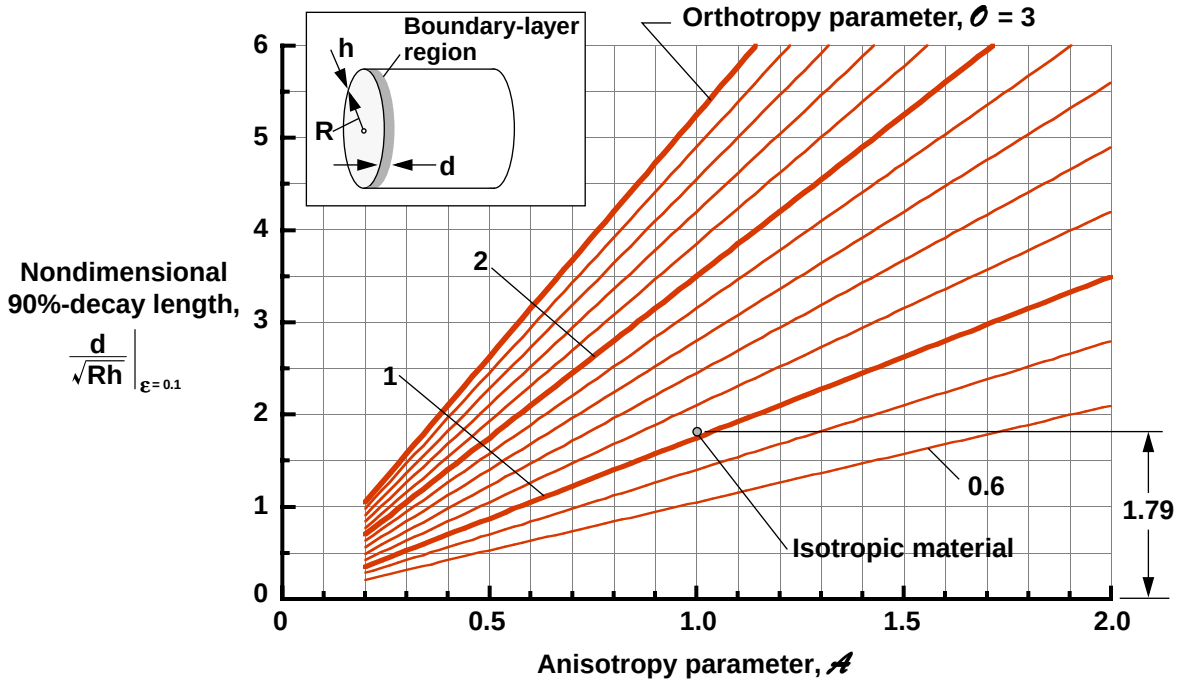

Figure 2. Nondimensional 90-percent-decay length for symmetrically and unsymmetrically laminated cylinders, as a function of laminate anisotropy.

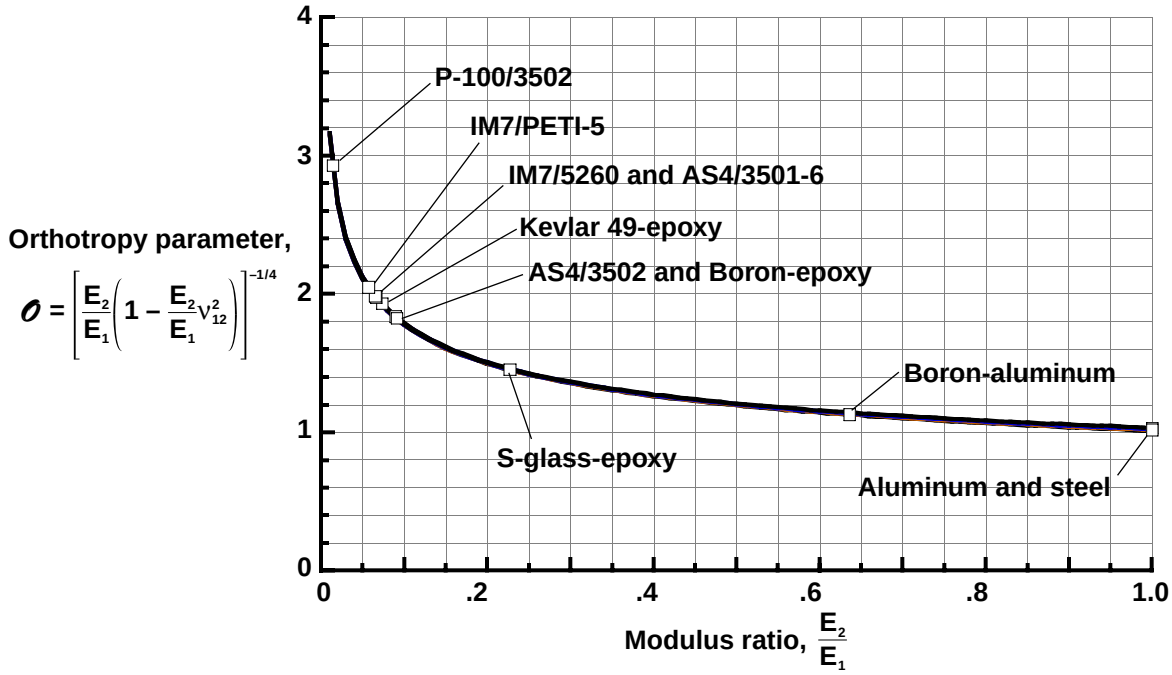

Figure 3. Effect of lamina material properties on nondimensional orthotropy parameter for single-ply, homogeneous, specially orthotropic laminates $(0.2 \le \nu_{12} \le 0.35)$.

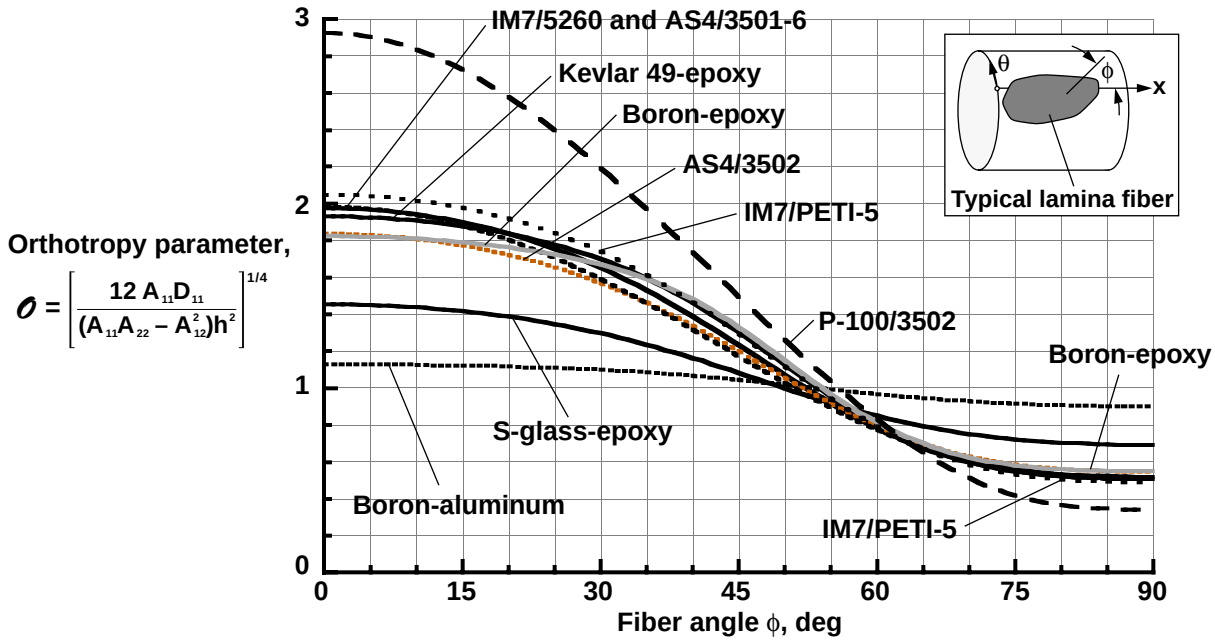

Figure 4. Effect of lamina material properties on nondimensional orthotropy parameter for $[(\pm\phi)_m]_s$, $[(+\phi)_{2m}]_s$, and $[(\pm\phi)_m]_T$ laminates (m = 1, 2, ...).

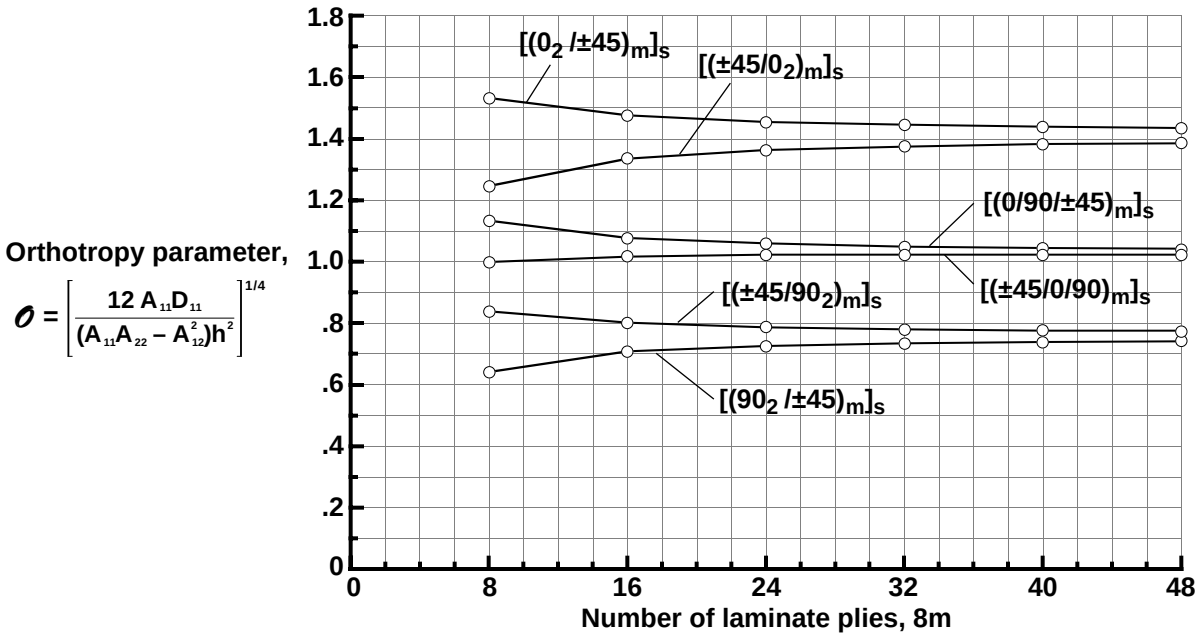

Figure 5. Nondimensional orthotropy parameter for typical laminates made of IM7/5260 material.

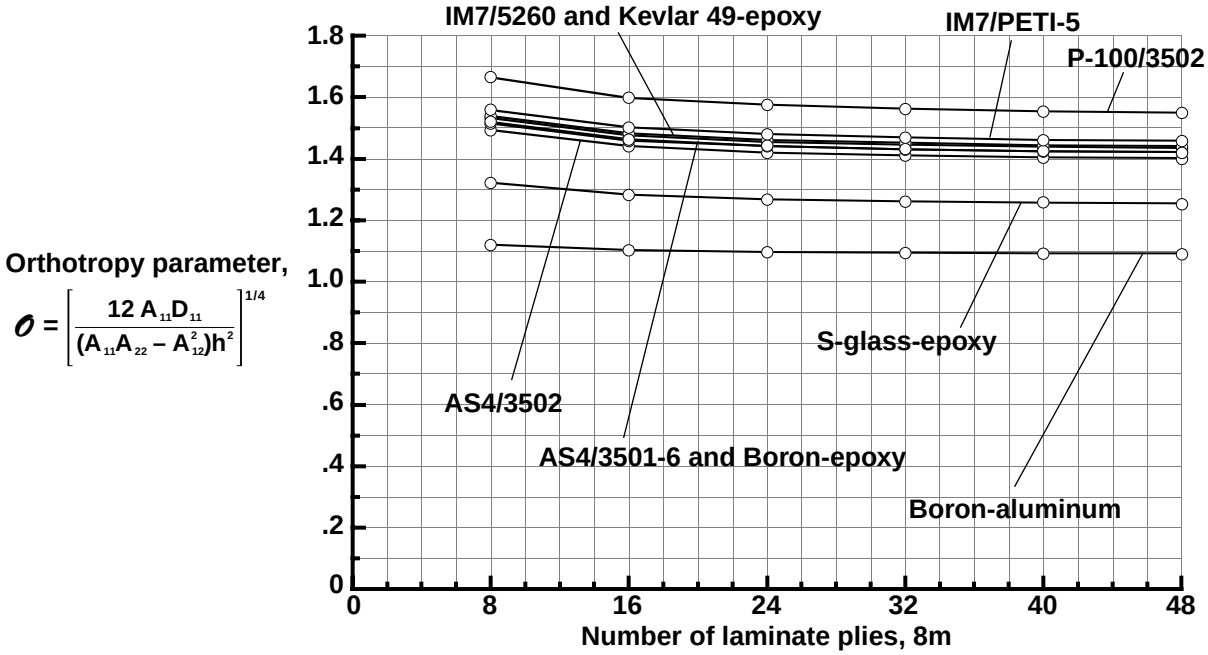

Figure 6. Effect of lamina material properties on nondimensional orthotropy parameter for $[(0_2/\pm45)_m]_s$ laminates.

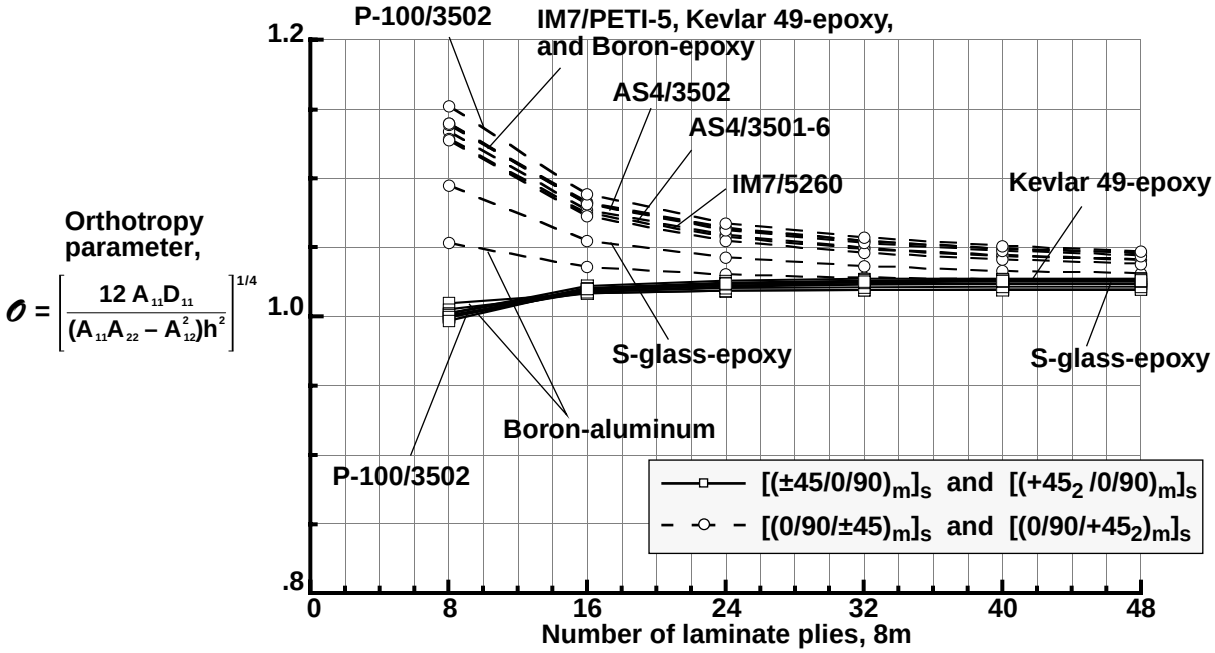

Figure 7. Effect of lamina material properties on nondimensional orthotropy parameter for quasi-isotropic laminates and similar unbalanced laminates.

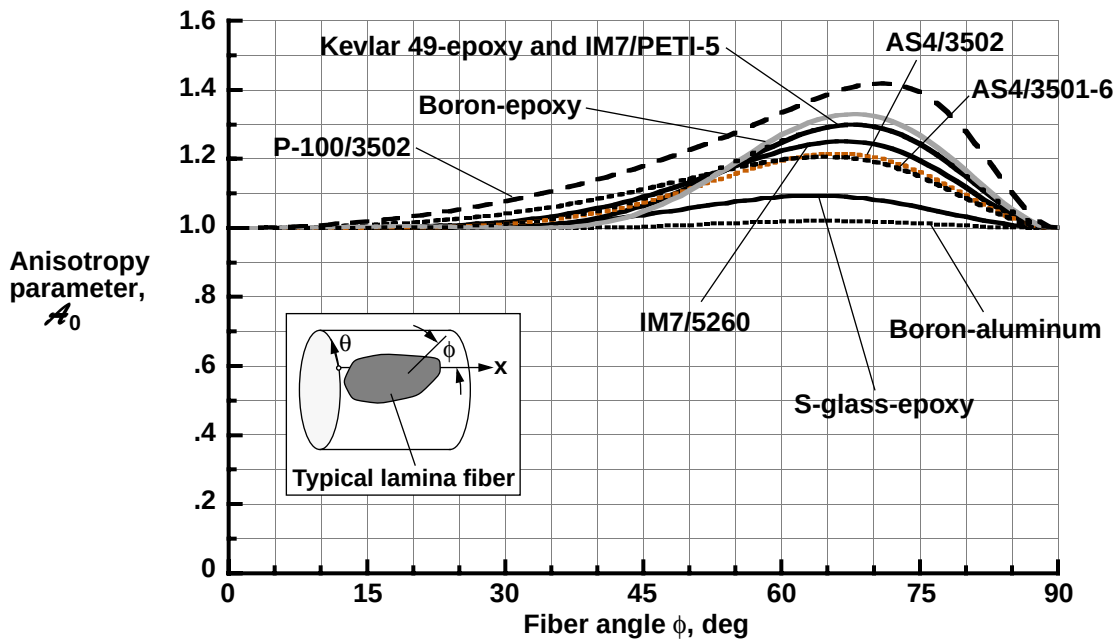

Figure 8. Effect of lamina material properties on nondimensional anisotropy parameter for $[(+\phi)_{2m}]_s$ laminates (m = 1, 2, ...).

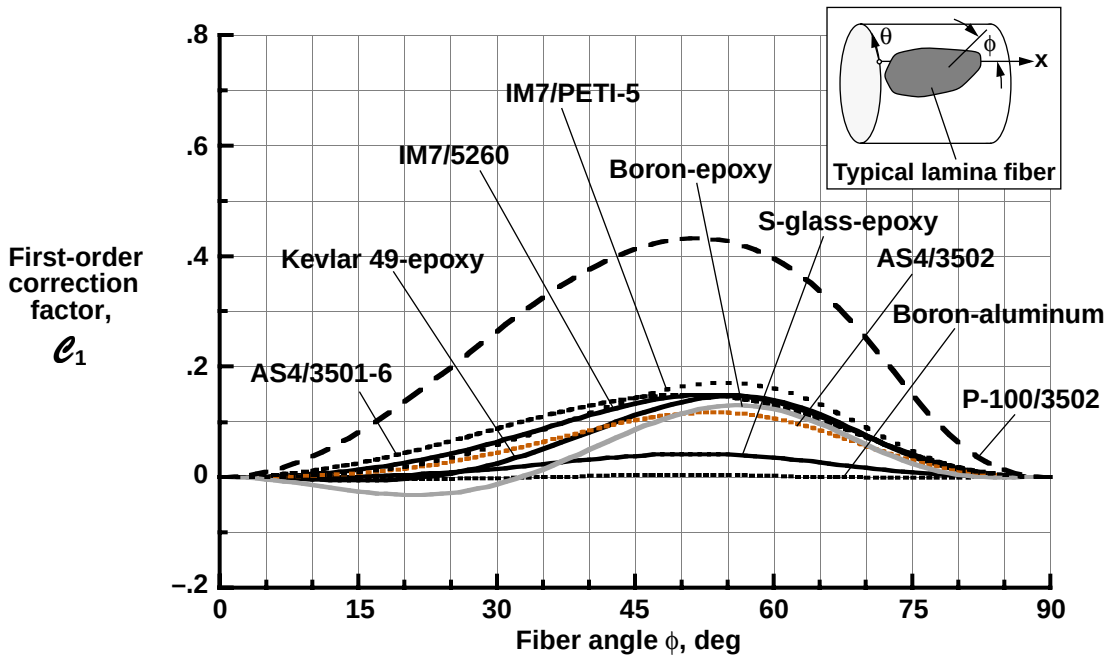

Figure 9. Effect of lamina material properties on nondimensional first-order correction factor for $[(+\phi)_{2m}]_s$ laminates (m = 1, 2, ...).

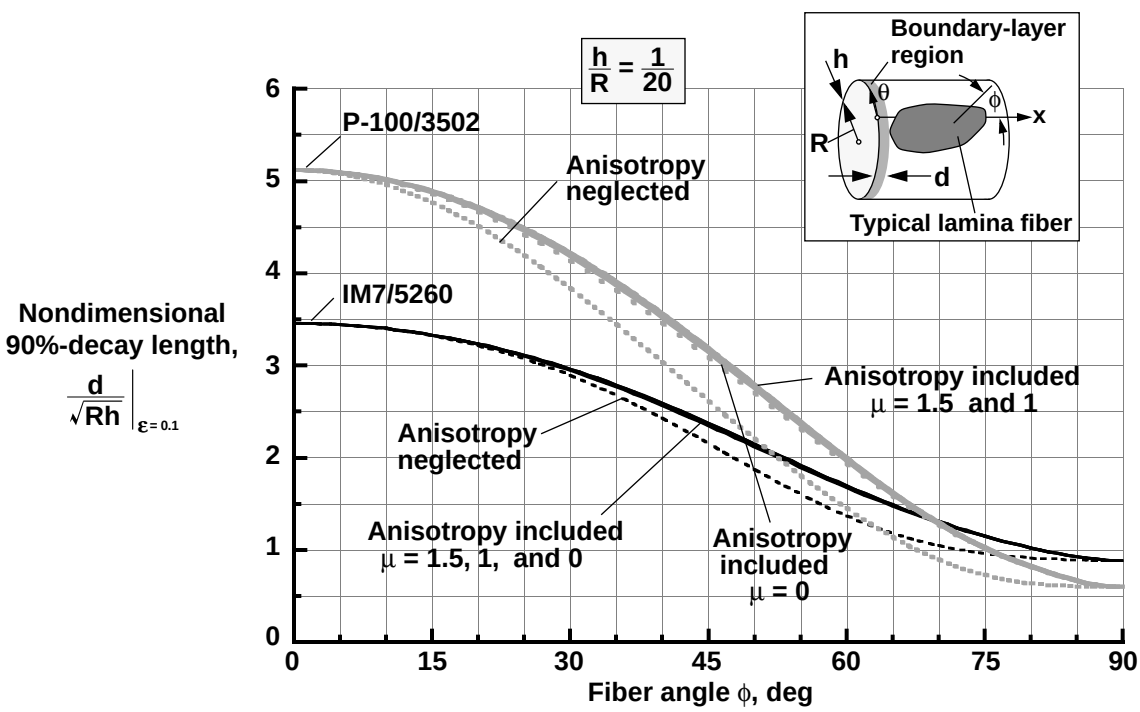

Figure 10. Nondimensional 90-percent-decay length for $[(+\phi)_{2m}]_s$ laminates made of IM7/5260 graphite-bismaleimide and P-100/3502 pitch-epoxy material $\left(\frac{h}{R} = \frac{1}{20}; m = 1, 2, \ldots\right)$.

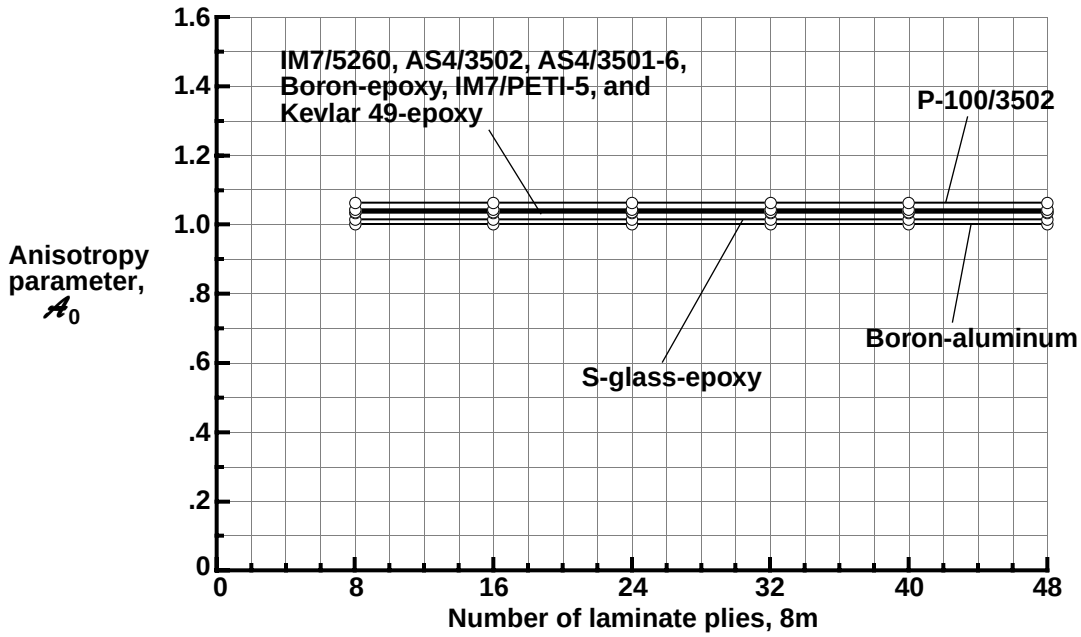

Figure 11. Effect of lamina material properties on nondimensional anisotropy parameter for $[(0/90/+45_2)_m]_s$ and $[(+45_2/0/90)_m]_s$ laminates.

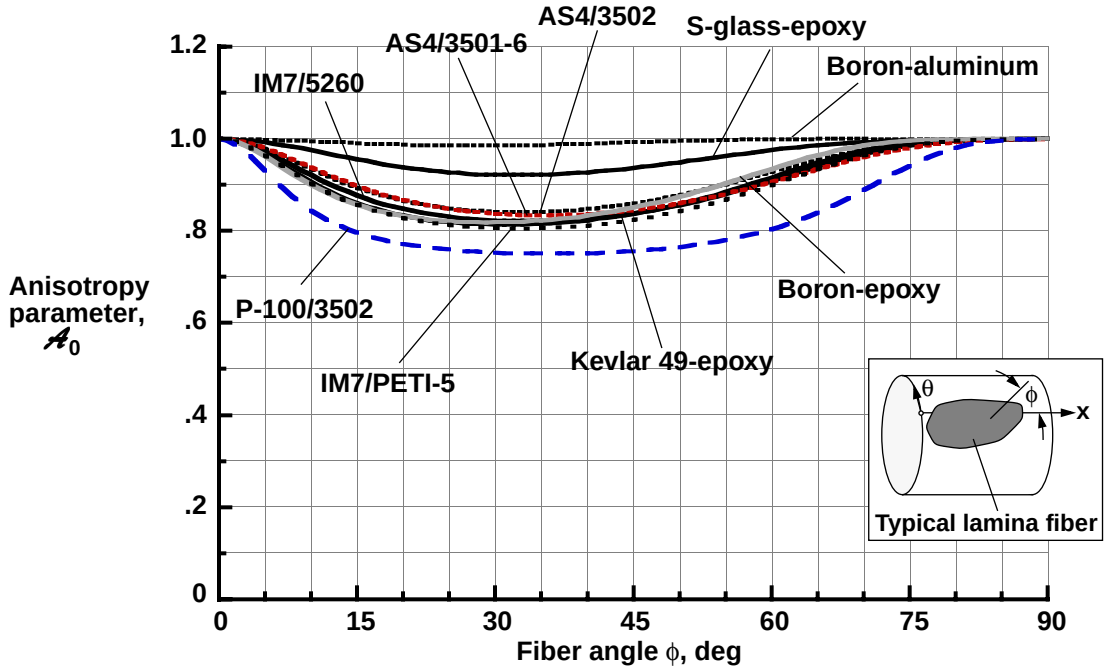

Figure 12. Effect of lamina material properties on nondimensional anisotropy parameter for $[\pm\phi]_T$ laminates.

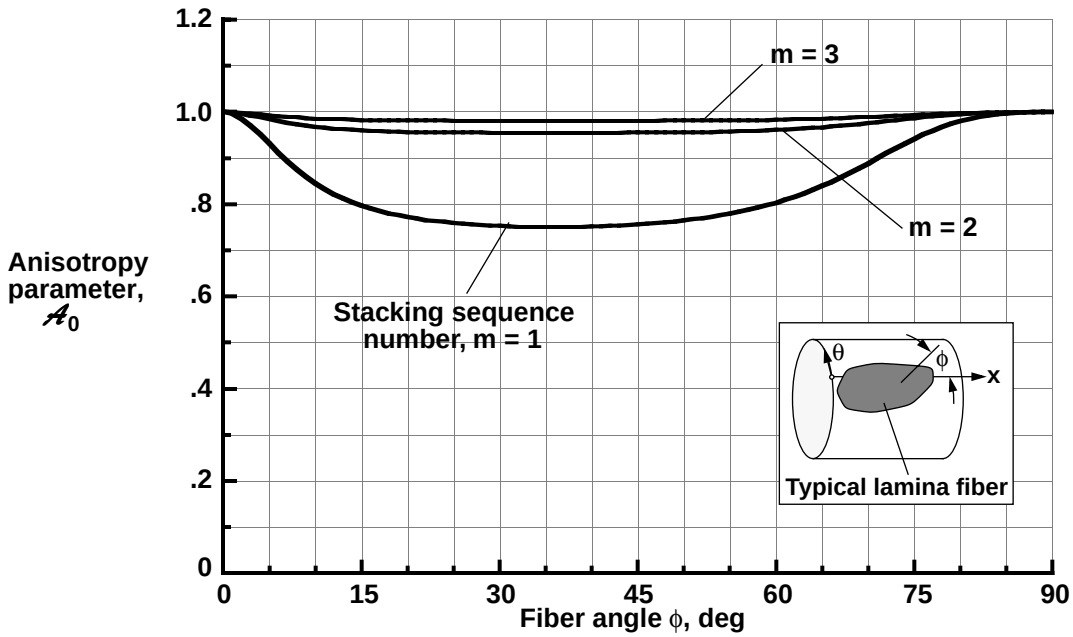

Figure 13. Effect of stacking sequence number on nondimensional anisotropy parameter for $[(\pm\phi)_m]_T$ laminates made of P-100/3502 pitch-epoxy material.

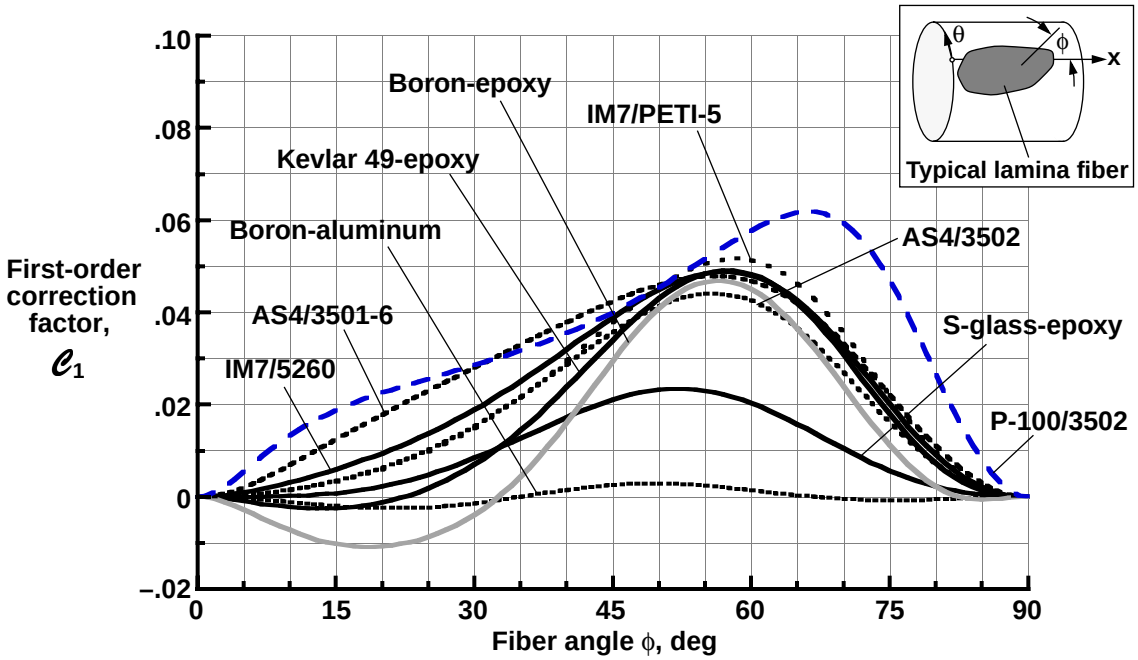

Figure 14. Effect of lamina material properties on nondimensional first-order correction factor for $[\pm\phi]_T$ laminates.

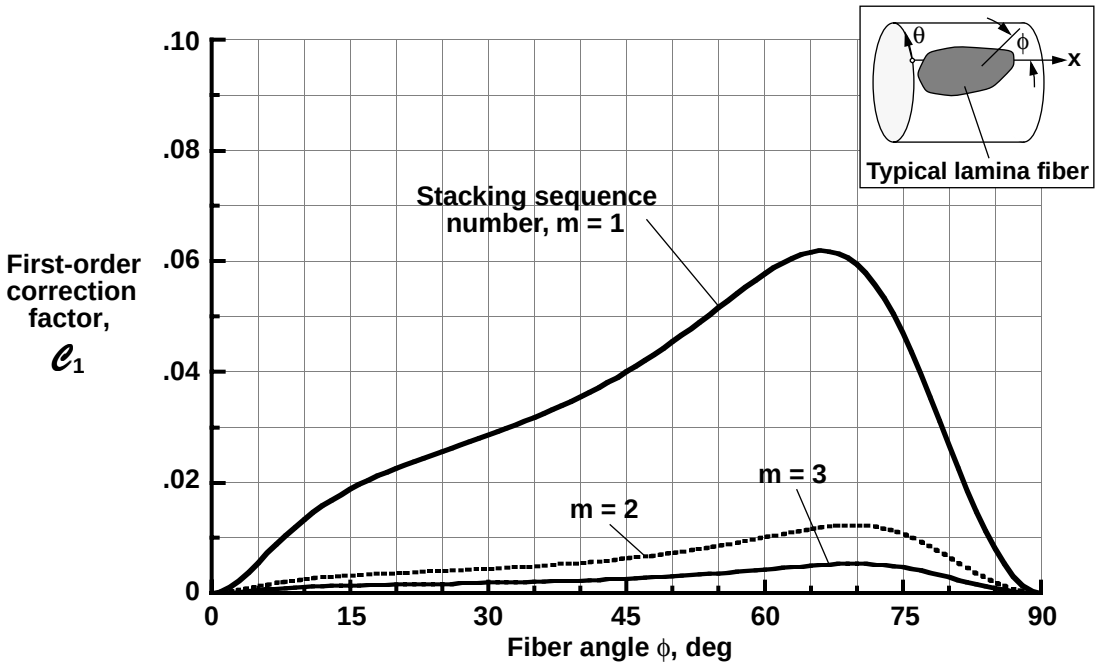

Figure 15. Effect of stacking sequence number on nondimensional first-order correction factor for $[(\pm\phi)_m]_T$ laminates made of P-100/3502 pitch-epoxy material.

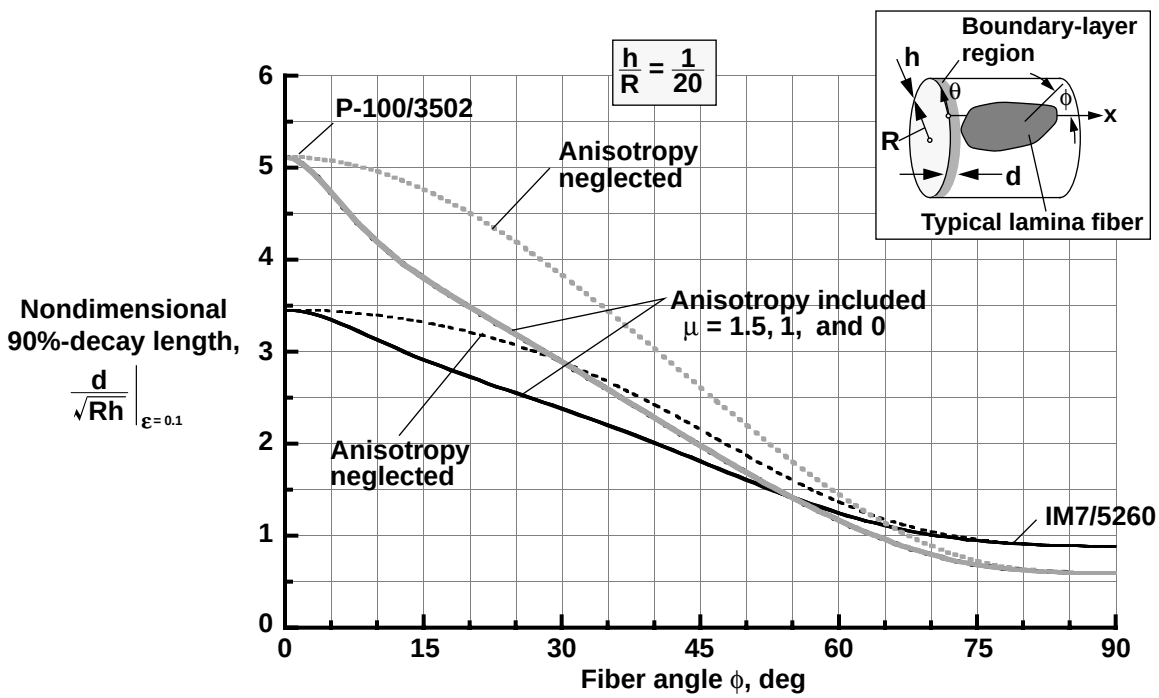

Figure 16. Nondimensional 90-percent-decay length for $[\pm\phi]_T$ laminates made of IM7/5260 graphite-bismaleimide and P-100/3502 pitch-epoxy material $\left(\frac{h}{R} = \frac{1}{20}\right)$.

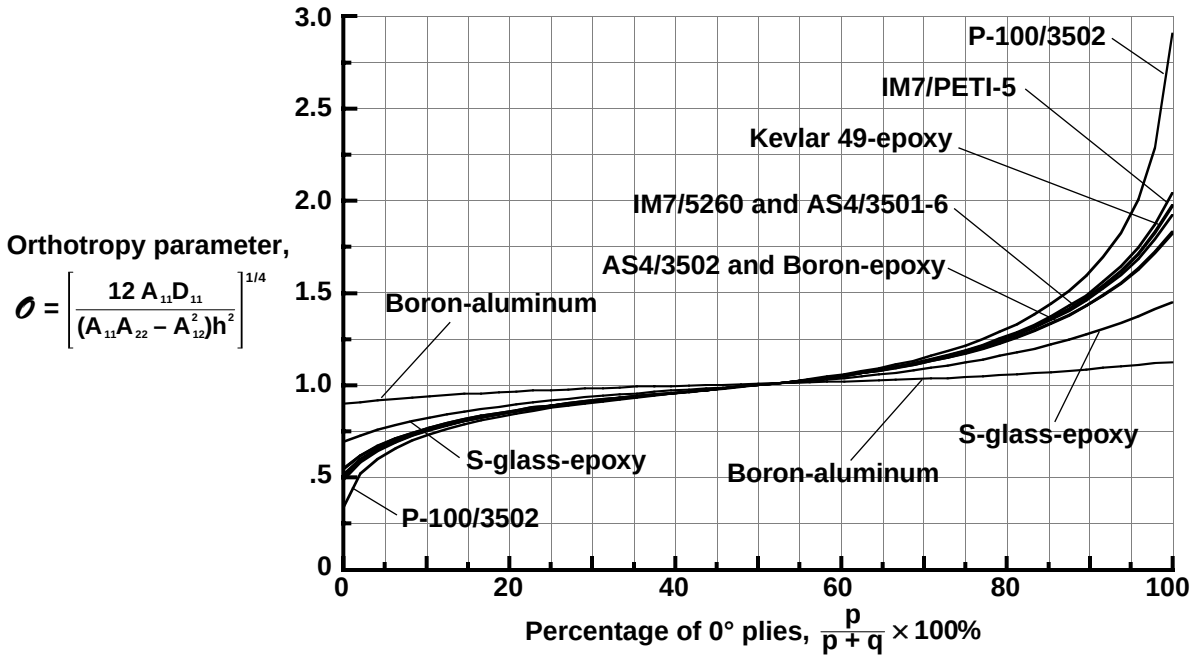

Figure 17. Effect of lamina material properties on nondimensional orthotropy parameter for $[0_p/90_q]_T$ laminates.

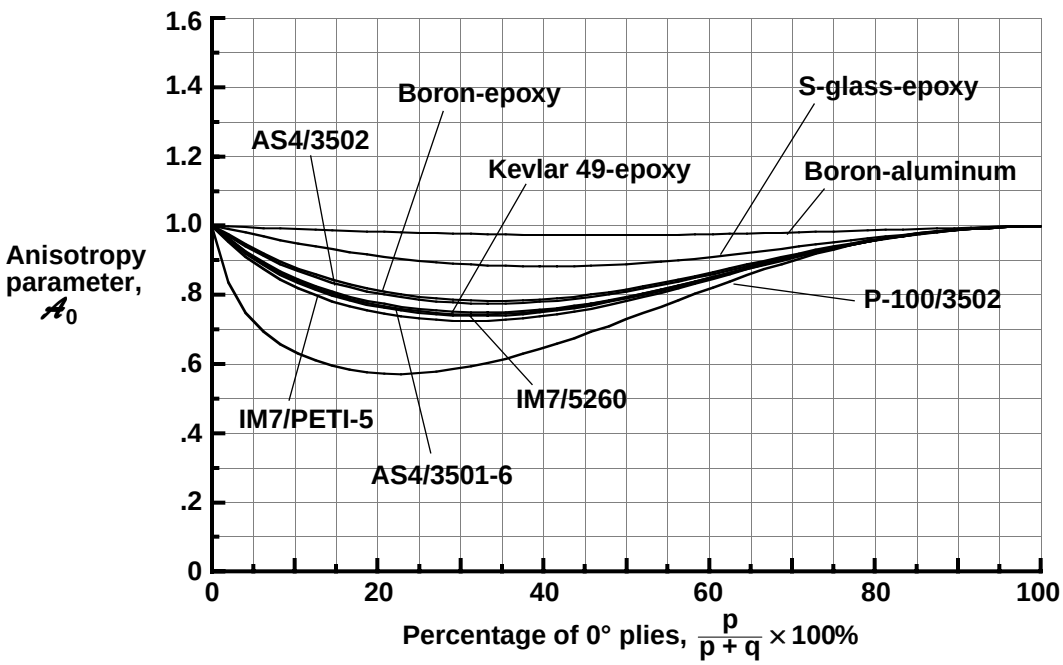

Figure 18. Effect of lamina material properties on nondimensional anisotropy parameter for $[0_p/90_q]_T$ laminates.

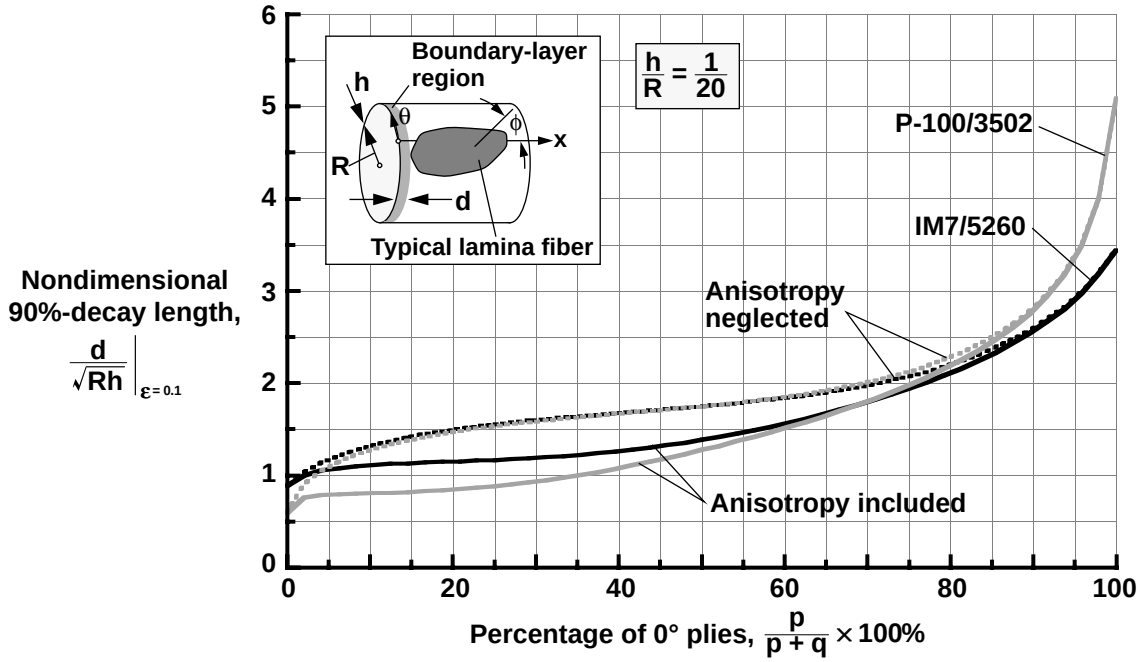

Figure 19. Nondimensional 90-percent-decay length for $[0_p/90_q]_T$ laminates made of IM7/5260 graphite-bismaleimide and P-100/3502 pitch-epoxy material $\left(\frac{h}{R} = \frac{1}{20}\right)$.

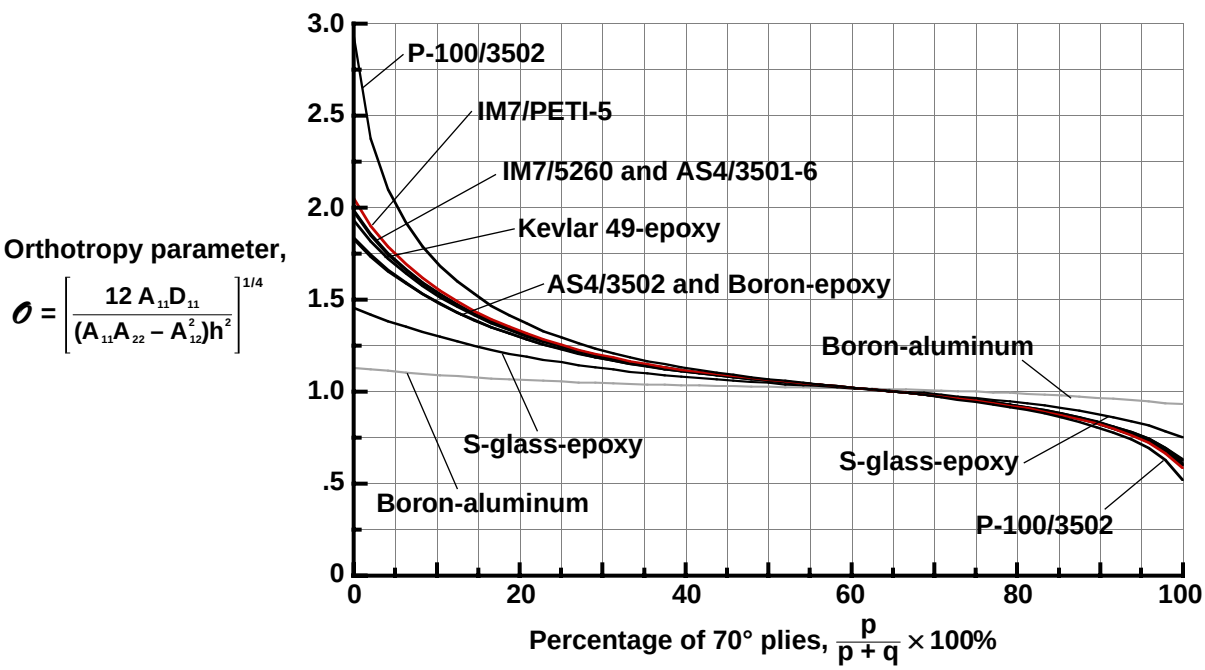

Figure 20. Effect of lamina material properties on nondimensional orthotropy parameter for $[70_p/0_q]_T$ laminates.

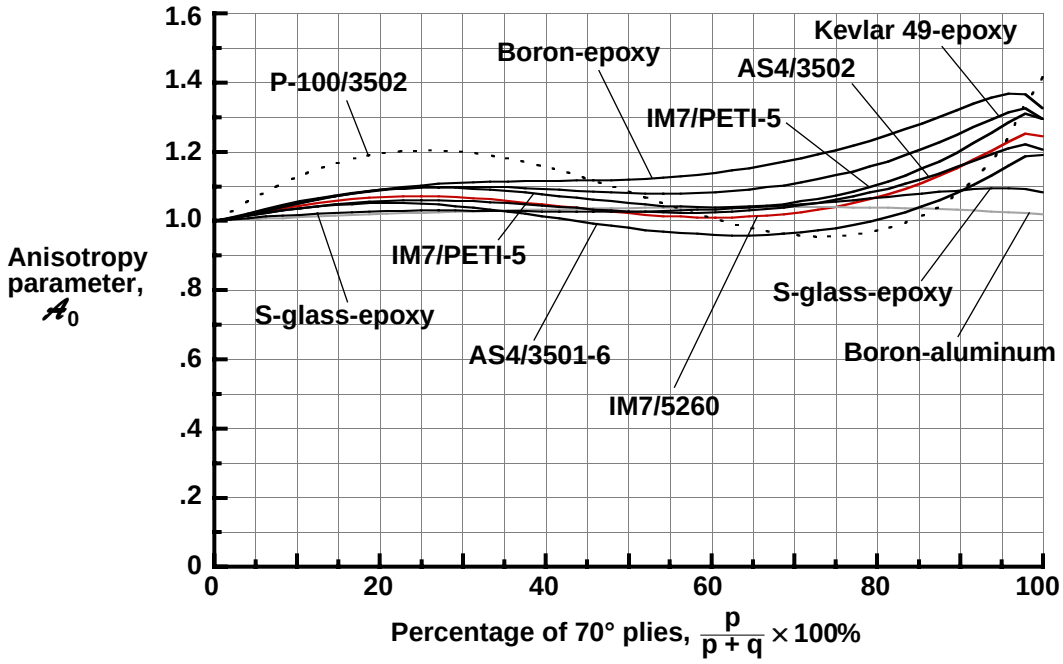

Figure 21. Effect of lamina material properties on nondimensional anisotropy parameter for $[70_p/0_q]_T$ laminates.

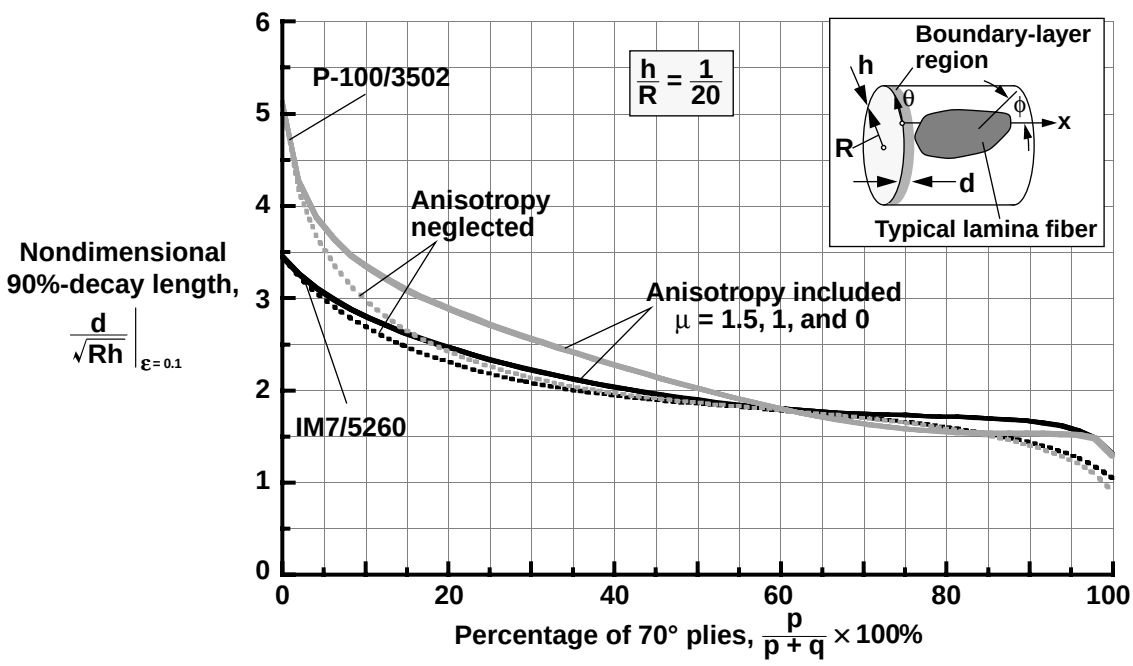

Figure 22. Nondimensional 90-percent-decay length for $[70_p/0_q]_T$ laminates made of IM7/5260 graphite-bismaleimide and P-100/3502 pitch-epoxy material $\left(\frac{h}{R} = \frac{1}{20}\right)$.

Appendix A

Sanders-Koiter Equations

The linear Sanders-Koiter shell equations (refs. 16 and 17) are presented in this appendix for a right-circular cylinder with a radius that is given by R. For these equations, x and θ denote the axial and circumferential coordinates, respectively. First, the equilibrium equations are presented; then the kinematic equations and the constitutive equations are presented. Last, the boundary conditions are given for a complete right-circular cylinder at an edge that is given by a constant value of the axial coordinate x.

Equilibrium Equations

The equilibrium equations are given in a form similar to those found in reference 22; that is,

$$\frac{\partial N_x}{\partial x} + \frac{1}{R}\frac{\partial N_{x\theta}}{\partial \theta} - \frac{c_2}{2R^2}\frac{\partial M_{x\theta}}{\partial \theta} + q_x = 0 \tag{A1}$$

$$\frac{\partial N_{x\theta}}{\partial x} + \frac{1}{R}\frac{\partial N_\theta}{\partial \theta} + \frac{c_1}{R}Q_\theta + \frac{c_2}{2R}\frac{\partial M_{x\theta}}{\partial x} + q_\theta = 0 \tag{A2}$$

$$\frac{\partial Q_x}{\partial x} + \frac{1}{R}\frac{\partial Q_\theta}{\partial \theta} - \frac{N_\theta}{R} + q_n = 0 \tag{A3}$$

$$\frac{\partial M_x}{\partial x} + \frac{1}{R}\frac{\partial M_{x\theta}}{\partial \theta} - Q_x = 0 \tag{A4}$$

$$\frac{\partial M_{x\theta}}{\partial x} + \frac{1}{R}\frac{\partial M_\theta}{\partial \theta} - Q_\theta = 0 \tag{A5}$$

where N_x, N_θ, and $N_{x\theta}$ are the membrane stress resultants; Q_x and Q_θ are the transverse shear-stress resultants; M_x, M_θ, and $M_{x\theta}$ are the bending stress resultants; q_x, q_θ, and q_n are the applied surface tractions; and c_1 and c_2 are constants that identify the equations of other shell theories that are considered herein. In particular, the Sanders-Koiter equations are given by $c_1 = c_2 = 1$, and the Love-Kirchhoff equations are given by $c_1 = 1$ and $c_2 = 0$. Donnell's equations are given by $c_1 = c_2 = 0$. This convention is used throughout the present study.

Kinematic Equations

The kinematic equations are given by

$$\varepsilon_x^o = \frac{\partial u}{\partial x} \tag{A6}$$

$$\varepsilon_\theta^o = \frac{1}{R}\frac{\partial v}{\partial \theta} + \frac{w}{R} \tag{A7}$$

$$\gamma_{x\theta}^o = \frac{\partial v}{\partial x} + \frac{1}{R}\frac{\partial u}{\partial \theta} \tag{A8}$$

$$\beta_x^o = -\frac{\partial w}{\partial x} \tag{A9}$$

$$\beta_\theta^o = \frac{c_1}{R} v - \frac{1}{R}\frac{\partial w}{\partial \theta} \tag{A10}$$

$$\beta_n^o = \frac{c_2}{2}\left(\frac{\partial v}{\partial x} - \frac{1}{R}\frac{\partial u}{\partial \theta}\right) \tag{A11}$$

$$\kappa_x^o = \frac{\partial \beta_x^o}{\partial x} = -\frac{\partial^2 w}{\partial x^2} \tag{A12}$$

$$\kappa_\theta^o = \frac{1}{R}\frac{\partial \beta_\theta^o}{\partial \theta} = \frac{c_1}{R^2}\frac{\partial v}{\partial \theta} - \frac{1}{R^2}\frac{\partial^2 w}{\partial \theta^2} \tag{A13}$$

$$\kappa_{x\theta}^o = \frac{1}{R}\left(\frac{\partial \beta_x^o}{\partial \theta} + \beta_n^o\right) + \frac{\partial \beta_\theta^o}{\partial x} = -\frac{2}{R}\frac{\partial^2 w}{\partial x \partial \theta} + \frac{1}{R}\left(c_1 + \frac{1}{2}c_2\right)\frac{\partial v}{\partial x} - \frac{c_2}{2R^2}\frac{\partial u}{\partial \theta} \tag{A14}$$

where u, v, and w are the axial, circumferential, and radial displacements of a point of the shell middle surface; ε_x^o, ε_θ^o, and $\gamma_{x\theta}^o$ are the membrane strains; β_x^o, β_θ^o, and β_n^o are the rotations; and κ_x^o, κ_θ^o, and $\kappa_{x\theta}^o$ are the bending strains. The displacement w is positive when it is outward from the cylinder reference surface.

Constitutive Equations

The isothermal constitutive equations are given in matrix form by

$$\begin{Bmatrix} N_x \\ N_\theta \\ N_{x\theta} \\ \hdashline M_x \\ M_\theta \\ M_{x\theta} \end{Bmatrix} = \left[\begin{array}{ccc:ccc} A_{11} & A_{12} & A_{16} & B_{11} & B_{12} & B_{16} \\ A_{12} & A_{22} & A_{26} & B_{12} & B_{22} & B_{26} \\ A_{16} & A_{26} & A_{66} & B_{16} & B_{26} & B_{66} \\ \hdashline B_{11} & B_{12} & B_{16} & D_{11} & D_{12} & D_{16} \\ B_{12} & B_{22} & B_{26} & D_{12} & D_{22} & D_{26} \\ B_{16} & B_{26} & B_{66} & D_{16} & D_{26} & D_{66} \end{array}\right] \begin{Bmatrix} \varepsilon_x^o \\ \varepsilon_\theta^o \\ \gamma_{x\theta}^o \\ \hdashline \kappa_x^o \\ \kappa_\theta^o \\ \kappa_{x\theta}^o \end{Bmatrix} \tag{A15}$$

where the subscripted A, B, and D terms of the matrix are the stiffnesses of laminated-composite shells that are obtained from the Love-Kirchhoff shell theory. Moreover, the constitutive terms in equation (A15) are identical to those for laminated-composite plates that are given in reference 18, page 198.

Boundary Conditions

The boundary conditions for an edge that is defined by a constant value of the axial coordinate x are given by

$$N_x = \tilde{N}_x(\theta) \quad \text{or} \quad u = \tilde{u}(\theta) \tag{A16}$$

$$N_{x\theta} + \frac{1}{R}\left(c_1 + \frac{1}{2}c_2\right)M_{x\theta} = \tilde{T}(\theta) \quad \text{or} \quad v = \tilde{v}(\theta) \tag{A17}$$

$$Q_x + \frac{1}{R}\frac{\partial M_{x\theta}}{\partial \theta} = \tilde{V}(\theta) \quad \text{or} \quad w = \tilde{w}(\theta) \tag{A18}$$

$$M_x = \tilde{M}_x(\theta) \quad \text{or} \quad \beta_x^o = \tilde{\beta}(\theta) \tag{A19}$$

where $\tilde{u}(\theta)$, $\tilde{v}(\theta)$, and $\tilde{w}(\theta)$ are applied edge displacements; $\tilde{\beta}(\theta)$ is an applied edge rotation; and $\tilde{N}_x(\theta)$, $\tilde{T}(\theta)$, $\tilde{V}(\theta)$, and $\tilde{M}_x(\theta)$ are applied edge loads.

Appendix B

Equations for Axisymmetry

The linear Sanders-Koiter shell equations that are presented in appendix A for a right-circular cylinder with a radius R are specialized in this appendix for the case of axisymmetric behavior. For these equations, x and θ denote the axial and circumferential coordinates, respectively. The specialization to axial symmetry is conducted by eliminating all terms in the equations of appendix A that are differentiated with respect to the circumferential coordinate θ. First, the equilibrium equations, the kinematic equations, and the constitutive equations are presented. Then, the boundary conditions are given for a complete right-circular cylinder at an edge that is given by a constant value of the axial coordinate x. Last, the axisymmetric equations are manipulated into a single ordinary differential equation in terms of the radial displacement $w(x)$.

Equilibrium Equations

The equilibrium equations for axisymmetric behavior are given by

$$\frac{dN_x}{dx} + q_x(x) = 0 \tag{B1}$$

$$\frac{dN_{x\theta}}{dx} + \frac{c_1}{R} Q_\theta + \frac{c_2}{2R} \frac{dM_{x\theta}}{dx} + q_\theta(x) = 0 \tag{B2}$$

$$\frac{dQ_x}{dx} - \frac{N_\theta}{R} + q_n(x) = 0 \tag{B3}$$

$$\frac{dM_x}{dx} - Q_x = 0 \tag{B4}$$

$$\frac{dM_{x\theta}}{dx} - Q_\theta = 0 \tag{B5}$$

where the membrane stress resultants N_x, N_θ, and $N_{x\theta}$; the transverse shear-stress resultants Q_x and Q_θ; the bending stress resultants M_x, M_θ, and $M_{x\theta}$; and the applied surface tractions q_x, q_θ, and q_n are functions of only the axial coordinate x.

Kinematic Equations

The kinematic equations are given by

$$\varepsilon_x^o = \frac{du}{dx} \tag{B6}$$

$$\varepsilon_\theta^o = \frac{w}{R} \tag{B7}$$

$$\gamma_{x\theta}^o = \frac{dv}{dx} \tag{B8}$$

$$\beta_x^o = -\frac{dw}{dx} \tag{B9}$$

$$\beta_\theta^o = \frac{c_1}{R} v \tag{B10}$$

$$\beta_n^o = \frac{c_2}{2} \frac{dv}{dx} \tag{B11}$$

$$\kappa_x^o = \frac{d\beta_x^o}{dx} = -\frac{d^2 w}{dx^2} \tag{B12}$$

$$\kappa_\theta^o = 0 \tag{B13}$$

$$\kappa_{x\theta}^o = \frac{1}{R} \beta_n^o + \frac{d\beta_\theta^o}{dx} = \frac{1}{R}\left(c_1 + \frac{1}{2} c_2\right)\frac{dv}{dx} \tag{B14}$$

where the middle-surface displacements u, v, and w; the membrane strains ε_x^o, ε_θ^o, and $\gamma_{x\theta}^o$; the rotations β_x^o, β_θ^o, and β_n^o; and the bending strains κ_x^o, κ_θ^o, and $\kappa_{x\theta}^o$ are functions of only the axial coordinate x.

Constitutive Equations

The isothermal constitutive equations reduce to

$$\begin{Bmatrix} N_x \\ N_\theta \\ N_{x\theta} \\ \hdashline M_x \\ M_\theta \\ M_{x\theta} \end{Bmatrix} = \left[\begin{array}{ccc:ccc} A_{11} & A_{12} & A_{16} & B_{11} & B_{12} & B_{16} \\ A_{12} & A_{22} & A_{26} & B_{12} & B_{22} & B_{26} \\ A_{16} & A_{26} & A_{66} & B_{16} & B_{26} & B_{66} \\ \hdashline B_{11} & B_{12} & B_{16} & D_{11} & D_{12} & D_{16} \\ B_{12} & B_{22} & B_{26} & D_{12} & D_{22} & D_{26} \\ B_{16} & B_{26} & B_{66} & D_{16} & D_{26} & D_{66} \end{array}\right] \begin{Bmatrix} \varepsilon_x^o \\ \varepsilon_\theta^o \\ \gamma_{x\theta}^o \\ \hdashline \kappa_x^o \\ 0 \\ \kappa_{x\theta}^o \end{Bmatrix} \tag{B15}$$

where the subscripted A, B, and D terms of the matrix are the usual constitutive terms of classical Love-Kirchhoff-type laminated composite shell theory or classical laminated plate theory (e.g., see p. 198 of ref. 18).

Boundary Conditions

The boundary conditions for an edge that is defined by a constant value of the axial coordinate x are given by

$$N_x = \tilde{N}_x \quad \text{or} \quad u = \tilde{u} \tag{B16}$$

$$N_{x\theta} + \frac{1}{R}\left(c_1 + \frac{1}{2}c_2\right)M_{x\theta} = \tilde{T} \quad \text{or} \quad v = \tilde{v} \tag{B17}$$

$$Q_x = \tilde{V} \quad \text{or} \quad w = \tilde{w} \tag{B18}$$

$$M_x = \tilde{M}_x \quad \text{or} \quad \beta_x^o = \tilde{\beta} \tag{B19}$$

where the applied edge displacements $\tilde{u}$, $\tilde{v}$, and $\tilde{w}$; the applied edge rotation $\tilde{\beta}$; and the applied edge loads $\tilde{N}_x$, $\tilde{T}$, $\tilde{V}$, and $\tilde{M}_x$ are all constants.

Bending Boundary-Layer Equation

The bending boundary-layer equation is obtained by first noting that integration of equation (B1) yields

$$N_x = -\int q_x\,dx + C \equiv \bar{N}(x) \tag{B20}$$

where C is a constant of integration that is determined from the boundary condition given by equation (B16). Next, equations (B2) and (B5) are combined to get

$$\frac{dN_{x\theta}}{dx} + \frac{1}{R}\left(c_1 + \frac{1}{2}c_2\right)\frac{dM_{x\theta}}{dx} + q_\theta(x) = 0 \tag{B21}$$

For convenience, the parameter

$$\mu = c_1 + \frac{1}{2}c_2 \tag{B22}$$

is introduced such that the Sanders-Koiter equations are given by $\mu = \frac{3}{2}$ and the Love-Kirchhoff equations are given by $\mu = 1$. Donnell's equations are given by $\mu = 0$. Similarly, the function

$$\hat{T}(x) = N_{x\theta} + \frac{\mu}{R} M_{x\theta} \tag{B23}$$

is introduced so that equation (B21) becomes

$$\frac{d\hat{T}}{dx} + q_\theta(x) = 0 \tag{B24}$$

and the corresponding boundary condition given by equation (B17) becomes

$$\hat{T} = \tilde{T} \quad \text{or} \quad v = \tilde{v} \tag{B25}$$

Integration of equation (B24) yields

$$\hat{T} = -\int q_\theta \, dx + C \equiv \bar{T}(x) \tag{B26}$$

where C is a constant of integration that is determined from the boundary condition given by equation (B25). Next, equations (B3) and (B4) are combined to give

$$\frac{d^2 M_x}{dx^2} - \frac{N_\theta}{R} + q_n(x) = 0 \tag{B27}$$

The next step in the analysis is the simplification of the constitutive equations. First, by using equations (B8) and (B22), equation (B14) is expressed as

$$\kappa^o_{x\theta} = \frac{\mu}{R} \gamma^o_{x\theta} \tag{B28}$$

By using equations (B23) and (B28), the constitutive equations are expressed as

$$\begin{Bmatrix} N_x \\ N_\theta \\ \hat{T} \\ M_x \end{Bmatrix} = \begin{bmatrix} A_{11} & A_{12} & \bar{A}_{16} & B_{11} \\ A_{12} & A_{22} & \bar{A}_{26} & B_{12} \\ \bar{A}_{16} & \bar{A}_{26} & \bar{A}_{66} & \bar{B}_{16} \\ B_{11} & B_{12} & \bar{B}_{16} & D_{11} \end{bmatrix} \begin{Bmatrix} \varepsilon^o_x \\ \varepsilon^o_\theta \\ \gamma^o_{x\theta} \\ \kappa^o_x \end{Bmatrix} \tag{B29}$$

and

$$M_\theta = B_{12}\varepsilon^o_x + B_{22}\varepsilon^o_\theta + \bar{B}_{26}\gamma^o_{x\theta} + D_{12}\kappa^o_x \tag{B30}$$

where

$$\bar{A}_{16} = A_{16} + \mu\left(\frac{h}{R}\right)\frac{B_{16}}{h} \tag{B31}$$

$$\bar{A}_{26} = A_{26} + \mu\left(\frac{h}{R}\right)\frac{B_{26}}{h} \tag{B32}$$

$$\bar{A}_{66} = A_{66} + 2\mu\left(\frac{h}{R}\right)\frac{B_{66}}{h} + \mu^2\left(\frac{h}{R}\right)^2\frac{D_{66}}{h^2} \tag{B33}$$

$$\bar{B}_{16} = B_{16} + \mu\left(\frac{h}{R}\right)\frac{D_{16}}{h} \tag{B34}$$

$$\bar{B}_{26} = B_{26} + \mu\left(\frac{h}{R}\right)\frac{D_{26}}{h} \tag{B35}$$

The motivation for writing the constitutive equations in this form is that the matrix equation given by equation (B29) is the only part of the full constitutive equations that appears in the strain-energy density function, which is used in the present paper to determine the corresponding positive-definiteness conditions. With these simplified constitutive equations and equations (B6)–(B8) and (B12), equation (B20) is expressed as

$$A_{11}\frac{du}{dx} + A_{12}\frac{w}{R} + \bar{A}_{16}\frac{dv}{dx} - B_{11}\frac{d^2w}{dx^2} - \bar{N}(x) = 0 \tag{B36}$$

and equation (B26) is expressed as

$$\bar{A}_{16}\frac{du}{dx} + \bar{A}_{26}\frac{w}{R} + \bar{A}_{66}\frac{dv}{dx} - \bar{B}_{16}\frac{d^2w}{dx^2} - \bar{T}(x) = 0 \tag{B37}$$

Equations (B36) and (B37) are then solved for $\frac{du}{dx}$ and $\frac{dv}{dx}$ to get

$$\frac{du}{dx} = \frac{\bar{A}_{66}\bar{N}(x) - \bar{A}_{16}\bar{T}(x) + \left(\bar{A}_{16}\bar{A}_{26} - A_{12}\bar{A}_{66}\right)\frac{w}{R} + \left(\bar{A}_{66}B_{11} - \bar{A}_{16}\bar{B}_{16}\right)\frac{d^2w}{dx^2}}{A_{11}\bar{A}_{66} - \bar{A}_{16}^2} \tag{B38}$$

$$\frac{dv}{dx} = \frac{A_{11}\bar{T}(x) - \bar{A}_{16}\bar{N}(x) + \left(A_{12}\bar{A}_{16} - A_{11}\bar{A}_{26}\right)\frac{w}{R} + \left(A_{11}\bar{B}_{16} - \bar{A}_{16}B_{11}\right)\frac{d^2w}{dx^2}}{A_{11}\bar{A}_{66} - \bar{A}_{16}^2} \tag{B39}$$

Equation (B39) indicates that the circumferential displacement v(x) becomes uncoupled from the axial displacement u(x) and the radial displacement w(x) when $\bar{A}_{16} = \bar{A}_{26} = \bar{B}_{16} = 0$, which implies that $A_{16} = A_{26} = B_{16} = D_{16} = 0$. In addition, the constitutive equation (B29) indicates that N_x, N_θ, and M_x become uncoupled from the torsional, shear strain $\gamma^o_{x\theta}$ when $\bar{A}_{16} = \bar{A}_{26} = \bar{B}_{16} = 0$ and that $\hat{T}$, which is defined by equation (B23), becomes uncoupled from ε^o_x, ε^o_θ, and κ^o_x. Furthermore, equation (B30) indicates that M_θ becomes uncoupled from $\gamma^o_{x\theta}$ when $\bar{B}_{26} = 0$, which implies $B_{26} = D_{26} = 0$.

Next, equations (B38) and (B39) are then substituted into equations (B6) and (B8), and the resulting expressions for ε^o_x and $\gamma^o_{x\theta}$, along with equations (B7) and (B12), are substituted into the constitutive equation (B29). This action converts the strains and stress results in equation (B29) into functions of the radial displacement w(x). Substituting the expressions for N_θ and M_x into equation (B27) yields the bending boundary-layer equation that is given by

$$C_1 \frac{d^4 w}{dx^4} + C_2 \frac{d^2 w}{dx^2} + C_3 w = C_4(x) \tag{B40}$$

The constant coefficients are given by

$$C_1 = D_{11}\left[1 - \frac{\bar{A}_{66}B_{11}^2 + A_{11}\bar{B}_{16}^2 - 2\bar{A}_{16}B_{11}\bar{B}_{16}}{\left(A_{11}\bar{A}_{66} - \bar{A}_{16}^2\right)D_{11}}\right] \tag{B41}$$

$$C_2 = -\frac{2}{R}\left[B_{12} + \frac{\left(\bar{A}_{16}\bar{A}_{26} - A_{12}\bar{A}_{66}\right)B_{11} + \left(A_{12}\bar{A}_{16} - A_{11}\bar{A}_{26}\right)\bar{B}_{16}}{A_{11}\bar{A}_{66} - \bar{A}_{16}^2}\right] \tag{B42}$$

$$C_3 = \frac{\left(A_{11}A_{22} - A_{12}^2\right)\bar{A}_{66} - A_{11}\bar{A}_{26}^2 - A_{22}\bar{A}_{16}^2 + 2A_{12}\bar{A}_{16}\bar{A}_{26}}{R^2\left(A_{11}\bar{A}_{66} - \bar{A}_{16}^2\right)} \tag{B43}$$

The function $C_4(x)$ is given by

$$C_4(x) = q_n(x) + \frac{\left(\bar{A}_{16}\bar{A}_{26} - A_{12}\bar{A}_{66}\right)\bar{N}(x) + \left(A_{12}\bar{A}_{16} - A_{11}\bar{A}_{26}\right)\bar{T}(x)}{R\left(A_{11}\bar{A}_{66} - \bar{A}_{16}^2\right)}$$

$$+ \frac{\left(B_{11}\bar{A}_{66} - \bar{A}_{16}\bar{B}_{16}\right)\frac{d^2\bar{N}}{dx^2} + \left(A_{11}\bar{B}_{16} - B_{11}\bar{A}_{16}\right)\frac{d^2\bar{T}}{dx^2}}{A_{11}\bar{A}_{66} - \bar{A}_{16}^2} \tag{B44}$$

These expressions are simplifed further by introducing the following expressions:

$$\bar{a}_{12} = \frac{\bar{A}_{16}\bar{A}_{26} - A_{12}\bar{A}_{66}}{\left(A_{11}A_{22} - A_{12}^2\right)\bar{A}_{66} - A_{11}\bar{A}_{26}^2 - A_{22}\bar{A}_{16}^2 + 2A_{12}\bar{A}_{16}\bar{A}_{26}} \tag{B45}$$

$$\bar{a}_{22} = \frac{A_{11}\bar{A}_{66} - \bar{A}_{16}^2}{\left(A_{11}A_{22} - A_{12}^2\right)\bar{A}_{66} - A_{11}\bar{A}_{26}^2 - A_{22}\bar{A}_{16}^2 + 2A_{12}\bar{A}_{16}\bar{A}_{26}} \tag{B46}$$

$$\bar{a}_{26} = \frac{A_{12}\bar{A}_{16} - A_{11}\bar{A}_{26}}{\left(A_{11}A_{22} - A_{12}^2\right)\bar{A}_{66} - A_{11}\bar{A}_{26}^2 - A_{22}\bar{A}_{16}^2 + 2A_{12}\bar{A}_{16}\bar{A}_{26}} \tag{B47}$$

$$\bar{b}_{21} = -\left(\bar{a}_{12}B_{11} + \bar{a}_{22}B_{12} + \bar{a}_{26}\bar{B}_{16}\right) \tag{B48}$$

$$\boldsymbol{e} = 1 - \frac{\bar{A}_{66}B_{11}^2 + A_{11}\bar{B}_{16}^2 - 2\bar{A}_{16}B_{11}\bar{B}_{16}}{\left(A_{11}\bar{A}_{66} - \bar{A}_{16}^2\right)D_{11}} \tag{B49}$$

By using equations (B45)–(B49), equations (B41)–(B43) are expressed as

$$C_1 = D_{11}\boldsymbol{e} \tag{B50}$$

$$C_2 = \frac{2}{R}\frac{\bar{b}_{21}}{\bar{a}_{22}} \tag{B51}$$

$$C_3 = \frac{1}{R^2\bar{a}_{22}} \tag{B52}$$

Similarly, for the case where the second derivatives of $\bar{N}(x)$ and $\bar{T}(x)$ are zero valued, equation (B44) becomes

$$C_4(x) = q_n(x) + \frac{\bar{a}_{12}\bar{N}(x) + \bar{a}_{26}\bar{T}(x)}{R\bar{a}_{22}} \tag{B53}$$

The desired form of the bending boundary-layer equation is obtained by dividing equation (B40) by C_1; that is,

$$\frac{d^4w}{dx^4} + 4S\frac{d^2w}{dx^2} + 4Qw = P(x) \tag{B54}$$

where the constants S and Q are given by

$$S = \frac{C_2}{4C_1} = \frac{\bar{b}_{21}}{2R\bar{a}_{22}D_{11}\mathscr{e}} \tag{B55}$$

$$Q = \frac{C_3}{4C_1} = \frac{1}{4R^2\bar{a}_{22}D_{11}\mathscr{e}} \tag{B56}$$

The function P(x) is given by

$$P(x) = \frac{C_4(x)}{C_1} = \frac{q_n(x)}{D_{11}\mathscr{e}} + \frac{\bar{a}_{12}\bar{N}(x) + \bar{a}_{26}\bar{T}(x)}{R\bar{a}_{22}D_{11}\mathscr{e}} \tag{B57}$$

for the special case when the second derivatives of $\bar{N}(x)$ and $\bar{T}(x)$ are zero valued. The quantity $D_{11}\mathscr{e}$ that appears in equations (B54)–(B56) is sometimes referred to, in some contexts, as a reduced bending stiffness (ref. 12).

Appendix C

Anisotropy-Factor Equations

The first-order approximation of the anisotropy factor $\mathcal{A}$ that is used herein is given by

$$\mathcal{A} \approx \mathcal{A}_0 \left[1 + \mu \mathcal{C}_1 \left(\frac{h}{R} \right) \right] \tag{C1}$$

where $\mathcal{A}_0$ is the value of equation (20b), with $\mu = 0$ in the terms with the overbars. This expression is given by

$$\mathcal{A}_0 = \left(\frac{A_{11}A_{22} - A_{12}^2}{A_{11}} a_{22} \mathcal{e}_0 \right)^{1/4} \left(1 - \frac{b_{21}}{\sqrt{a_{22} D_{11} \mathcal{e}_0}} \right)^{-1/2} \tag{C2}$$

which is the anisotropy factor that corresponds to Donnell's equations. The terms a_{22}, b_{21}, and $\mathcal{e}_0$ are given by

$$a_{12} = \frac{A_{16}A_{26} - A_{12}A_{66}}{\left(A_{11}A_{22} - A_{12}^2 \right) A_{66} - A_{11}A_{26}^2 - A_{22}A_{16}^2 + 2A_{12}A_{16}A_{26}} \tag{C3}$$

$$a_{22} = \frac{A_{11}A_{66} - A_{16}^2}{\left(A_{11}A_{22} - A_{12}^2 \right) A_{66} - A_{11}A_{26}^2 - A_{22}A_{16}^2 + 2A_{12}A_{16}A_{26}} \tag{C4}$$

$$a_{26} = \frac{A_{12}A_{16} - A_{11}A_{26}}{\left(A_{11}A_{22} - A_{12}^2 \right) A_{66} - A_{11}A_{26}^2 - A_{22}A_{16}^2 + 2A_{12}A_{16}A_{26}} \tag{C5}$$

$$b_{21} = -\left(a_{12}B_{11} + a_{22}B_{12} + a_{26}B_{16} \right) \tag{C6}$$

$$\mathcal{e}_0 = 1 - \frac{A_{66}B_{11}^2 + A_{11}B_{16}^2 - 2A_{16}B_{11}B_{16}}{\left(A_{11}A_{66} - A_{16}^2 \right) D_{11}} \tag{C7}$$

The term $\mathcal{e}_1$ is a first-order correction to the results that correspond to Donnell's equations and is given by

$$\mathcal{e}_1 = \frac{\sqrt{a_{22}D_{11}\mathcal{e}_0}\left(a_{22}\mathcal{e}_1 + a_{122}\mathcal{e}_0\right) + 2a_{22}\left(b_{121}\mathcal{e}_0 - b_{21}\mathcal{e}_1\right) - 2a_{122}b_{21}\mathcal{e}_0}{4a_{22}\mathcal{e}_0\left(\sqrt{a_{22}D_{11}\mathcal{e}_0} - b_{21}\right)} \tag{C8}$$

where

$$\mathcal{e}_1 = \frac{2\left(A_{16}B_{11} - A_{11}B_{16}\right)\left[D_{16}\left(A_{11}A_{66} - A_{16}^2\right) - B_{16}\left(B_{11}A_{66} + A_{11}B_{66}\right) + A_{16}\left(A_{11}B_{66} + B_{16}^2\right)\right]}{\left(A_{11}A_{66} - A_{16}^2\right)^2 D_{11}h} \tag{C9}$$

$$a_{112} = \frac{B_{16}f_{16} + B_{26}f_{26} + B_{66}f_{66}}{\left[\left(A_{11}A_{22} - A_{12}^2\right)A_{66} - A_{11}A_{26}^2 - A_{22}A_{16}^2 + 2A_{12}A_{16}A_{26}\right]^2 h} \tag{C10}$$

$$a_{122} = -2\,\frac{B_{16}g_{16} + B_{26}g_{26} + B_{66}g_{66}}{\left[\left(A_{11}A_{22} - A_{12}^2\right)A_{66} - A_{11}A_{26}^2 - A_{22}A_{16}^2 + 2A_{12}A_{16}A_{26}\right]^2 h} \tag{C11}$$

$$a_{126} = \frac{B_{16}h_{16} + B_{26}h_{26} + B_{66}h_{66}}{\left[\left(A_{11}A_{22} - A_{12}^2\right)A_{66} - A_{11}A_{26}^2 - A_{22}A_{16}^2 + 2A_{12}A_{16}A_{26}\right]^2 h} \tag{C12}$$

$$b_{121} = -\left(a_{112}B_{11} + a_{122}B_{12} + a_{126}B_{16} + \frac{a_{26}D_{16}}{h}\right) \tag{C13}$$

and

$$f_{16} = A_{26}\left(A_{16}^2A_{22} - A_{11}A_{26}^2\right) + A_{66}\left[A_{26}\left(A_{11}A_{22} + A_{12}^2\right) - 2A_{12}A_{22}A_{16}\right] \tag{C14}$$

$$f_{26} = A_{16}\left(A_{26}^2 A_{11} - A_{22}A_{16}^2\right) + A_{66}\left[A_{16}\left(A_{11}A_{22} + A_{12}^2\right) - 2A_{11}A_{12}A_{26}\right] \tag{C15}$$

$$f_{66} = 2\left(A_{12}A_{16} - A_{11}A_{26}\right)\left(A_{16}A_{22} - A_{12}A_{26}\right) \tag{C16}$$

$$g_{16} = \left(A_{12}A_{16} - A_{11}A_{26}\right)\left(A_{16}A_{26} - A_{12}A_{66}\right) \tag{C17}$$

$$g_{26} = \left(A_{12}A_{16} - A_{11}A_{26}\right)\left(A_{11}A_{66} - A_{16}^2\right) \tag{C18}$$

$$g_{66} = \left(A_{12}A_{16} - A_{11}A_{26}\right)^2 \tag{C19}$$

$$h_{16} = A_{12}A_{66}\left(A_{12}A_{66} - A_{12}^2\right) + A_{11}A_{26}\left(A_{12}A_{26} - A_{16}A_{22}\right) + A_{16}A_{22}\left(A_{12}A_{16} - A_{11}A_{26}\right) \tag{C20}$$

$$h_{26} = -A_{11}A_{66}\left(A_{11}A_{22} - A_{12}^2\right) + A_{16}^2\left(A_{11}A_{22} - 2A_{12}^2\right) + A_{11}A_{26}\left(2A_{12}A_{16} - A_{11}A_{26}\right) \tag{C21}$$

$$h_{66} = 2\left(A_{11}A_{26} - A_{12}A_{16}\right)\left(A_{11}A_{22} - A_{12}^2\right) \tag{C22}$$

Special Cases for $\mathcal{A}_0$ and $\mathcal{C}_1$

Simplifications to $\mathcal{A}_0$ and $\mathcal{C}_1$ are presented below for unbalanced and balanced, symmetric laminates and for balanced, unsymmetric laminates that include the subclasses of general antisymmetric laminates, antisymmetric cross-ply laminates, and antisymmetric angle-ply laminates.

Unbalanced and balanced symmetric laminates

For unbalanced, symmetric laminates, $A_{16} \neq 0$, $A_{26} \neq 0$, and $B_{11} = B_{12} = B_{22} = B_{16} = B_{26} = B_{66} = 0$. For this special case,

$$\mathcal{A}_0 = \left\{\frac{\left(A_{11}A_{22} - A_{12}^2\right)\left(A_{11}A_{66} - A_{16}^2\right)}{A_{11}\left[\left(A_{11}A_{22} - A_{12}^2\right)A_{66} - A_{11}A_{26}^2 - A_{22}A_{16}^2 + 2A_{12}A_{16}A_{26}\right]}\right\}^{1/4} \tag{C23}$$

which agrees with the corresponding equations given by Reuter (ref. 4), and

$$\mathcal{C}_1 = \frac{D_{16}\left(A_{12}A_{16} - A_{11}A_{26}\right)}{2h\left[\left(A_{11}A_{22} - A_{12}^2\right)A_{66} - A_{11}A_{26}^2 - A_{22}A_{16}^2 + 2A_{12}A_{16}A_{26}\right]^{1/2}\left[D_{11}\left(A_{11}A_{66} - A_{16}^2\right)\right]^{1/2}} \tag{C24}$$

For balanced, symmetric laminates, $A_{16} = A_{26} = 0$ in addition to the subscripted B-matrix constitutive terms. For this special case, $\mathcal{A}_0 = 1$ and $\mathcal{C}_1 = 0$.

Balanced, unsymmetric laminates

For balanced, unsymmetric laminates, $A_{16} = A_{26} = 0$, which yields the following simplified expressions:

$$\mathcal{e}_0 = 1 - \frac{B_{11}^2}{A_{11}D_{11}} - \frac{B_{16}^2}{A_{66}D_{11}} \tag{C25}$$

$$\Lambda = \frac{A_{11}B_{12} - A_{12}B_{11}}{\sqrt{A_{11}D_{11}(A_{11}A_{22} - A_{12}^2)\,\mathcal{e}_0}} \tag{C26}$$

$$\mathcal{A}_0 = \sqrt[4]{\mathcal{e}_0}\left(1 + \Lambda\right)^{-1/2} \tag{C27}$$

$$\mathcal{e}_1 = -2\,\frac{B_{16}}{A_{66}h}\left(\frac{D_{16}}{D_{11}} - \frac{B_{11}B_{16}}{A_{11}D_{11}} - \frac{B_{16}B_{66}}{A_{66}D_{11}}\right) \tag{C28}$$

$$\mathcal{C}_1 = \frac{1}{4(1+\Lambda)}\left[\frac{\mathcal{e}_1}{\mathcal{e}_0}(1 + 2\Lambda) + \frac{2B_{16}\left(A_{11}B_{26} - A_{12}B_{16}\right)}{A_{66}h\sqrt{A_{11}D_{11}\left(A_{11}A_{22} - A_{12}^2\right)\mathcal{e}_0}}\right] \tag{C29}$$

For the subclass of balanced, antisymmetric laminates, $D_{16} = D_{26} = 0$, in addition to the shear-extensional coupling terms, which yields the following simplification:

$$\mathcal{e}_1 = \frac{2B_{16}^2}{A_{66}D_{11}h}\left(\frac{B_{11}}{A_{11}} + \frac{B_{66}}{A_{66}}\right) \tag{C30}$$

that is applied to equation (C29). For the subclass of (balanced) antisymmetric cross-ply laminates, $B_{12} = B_{16} = B_{26} = B_{66} = 0$, $B_{22} = -B_{11}$, and $D_{16} = D_{26} = 0$ in addition to the shear-extensional coupling terms. For this special case, $\mathcal{C}_1 = 0$ and

$$\mathcal{A}_0 = \sqrt[4]{\mathcal{e}_0}\left[1 - \frac{A_{12}B_{11}}{\sqrt{A_{11}D_{11}(A_{11}A_{22} - A_{12}^2)\mathcal{e}_0}}\right]^{-1/2} \tag{C31}$$

where

$$\mathcal{e}_0 = 1 - \frac{B_{11}^2}{A_{11}D_{11}} \tag{C32}$$

For the subclass of balanced, antisymmetric angle-ply laminates, $B_{11} = B_{12} = B_{22} = B_{66} = 0$ and $D_{16} = D_{26} = 0$ in addition to the shear-extensional coupling terms. For this special case, $\mathcal{A}_0 = \sqrt[4]{\mathcal{e}_0}$ where

$$\mathcal{e}_0 = 1 - \frac{B_{16}^2}{A_{66}D_{11}} \tag{C33}$$

which agrees with the corresponding equations given by Reuter (ref. 4), and

$$\mathcal{C}_1 = \frac{B_{16}\left(A_{11}B_{26} - A_{12}B_{16}\right)}{2A_{66}h\sqrt{A_{11}D_{11}\left(A_{11}A_{22} - A_{12}^2\right)\mathcal{e}_0}} \tag{C34}$$

Further simplifications can be made to equations (C31) and (C32) for [0/90/.../90] antisymmetric-cross-ply-laminate shell walls with an even number of layers that have identical material properties. For these laminates, the plies are specially orthotropic, and their principal material directions are oriented at 0° and 90° to the cylinder axes in an alternating manner. In particular, the major principal axes of the odd-numbered and even-numbered plies are aligned with the x- and θ-axis, respectively, with the first ply in the stacking sequence located at the inner surface of the cylinder. Moreover, all odd-numbered plies have the same thickness, and all even-numbered plies have the same thickness, but these two thicknesses are, in general, different. The laminate stiffnesses are given in reference 18 (see pp. 224–226) in terms of the number of layers N, the thickness ratio M, the ratio of the principal elastic moduli $F = \frac{E_2}{E_1}$ (for which $0 < F \leq 1$), and the reduced, plane-stress lamina stiffnesses. The thickness ratio is defined by

$$M = \sum_{k=1,3,\ldots}^{N-1} t_{(k)} \div \sum_{k=2,4,\ldots}^{N} t_{(k)} = \frac{t_{(1)}}{t_{(2)}} \tag{C35}$$

where $t_{(k)}$ denotes the thickness of the kth ply and

$$h = \sum_{k=1,3,\ldots}^{N-1} t_{(k)} + \sum_{k=2,4,\ldots}^{N} t_{(k)} = \frac{N}{2}\left(t_{(1)} + t_{(2)}\right) \tag{C36}$$

is the total laminate thickness. For the antisymmetric cross-ply laminates, $t_{(1)}$ and $t_{(2)}$ are the thicknesses of the 0° and 90° layers, respectively. Substituting the nonzero laminate stiffness expressions for this class of antisymmetric cross-ply laminates that are given in reference 18 into equations (21), (C31), and (C32) yields

$$\mathcal{O} = \left\{ \frac{[1-(1-F)Q](M+1)(M+F)}{(M+F)(1+MF) - [(1+M)F\nu_{12}]^2} \right\}^{1/4} \tag{C37}$$

$$\mathcal{A}_0 = \sqrt[4]{\mathcal{e}_0}\left(1 + \frac{\sqrt{12}\, MF(1-F)\nu_{12}}{N\sqrt{[1-(1-F)Q](M+1)(M+F)\{(M+F)(1+MF) - [(M+1)F\nu_{12}]^2\}\mathcal{e}_0}} \right)^{-1/2} \tag{C38}$$

$$\mathcal{e}_0 = 1 - \frac{12M^2(1-F)^2}{N^2(M+1)^3(M+F)[1-(1-F)Q]} \tag{C39}$$

where

$$Q = \frac{1}{1+M} + \frac{8M(M-1)}{N^2(M+1)^3} \tag{C40}$$

and ν_{12} is the major Poisson's ratio. For the special, but practical, case of regular antisymmetric cross-ply lamination, all plies have the same thickness and equations (C37)–(C39) reduce to

$$\mathcal{O} = \left[1 - \left(\frac{2F\nu_{12}}{1+F} \right)^2 \right]^{-1/4} \tag{C41}$$

$$\mathcal{A}_0 = \sqrt[4]{\mathcal{e}_0}\left\{ 1 + \frac{\sqrt{12}\, \nu_{12} F(1-F)}{N(1+F)\sqrt{\left[(1+F)^2 - (2F\nu_{12})^2\right]\mathcal{e}_0}} \right\}^{-1/2} \tag{C42}$$

$$\mathcal{e}_0 = 1 - \frac{3}{N^2}\left(\frac{1-F}{1+F} \right)^2 \tag{C43}$$

Appendix D

Example

Numerical calculations of the nondimensional orthotropy and anisotropy parameters and the bending boundary-layer decay length are presented in this appendix for a $[(\pm 45)_2/30_4/(0/90)_2]_T$ unbalanced, unsymmetrically laminated cylinder with a radius R = 4 in. For this laminate, the ±45° plies and the 0° and 90° plies are made of the Kevlar 49-epoxy material given in table 1. The other plies are made of the AS4/3502 graphite-epoxy material given in table 1. All ply thicknesses are 0.005 in., and the total wall thickness is given by h = 0.06 in.

The laminate stiffnesses were calculated from the formulas given on page 198 of reference 18 and are given in matrix form by

$$\begin{bmatrix} A_{11} & A_{12} & A_{16} \\ & A_{22} & A_{26} \\ \text{Symmetric} & & A_{66} \end{bmatrix} = \begin{bmatrix} 4.1678 & 1.3051 & 1.0787 \\ & 2.4682 & 0.3932 \\ \text{Symmetric} & & 1.4022 \end{bmatrix} \times 10^5 \text{ lb/in.}$$

$$\begin{bmatrix} B_{11} & B_{12} & B_{16} \\ & B_{22} & B_{26} \\ \text{Symmetric} & & B_{66} \end{bmatrix} = \begin{bmatrix} 0.7475 & -1.0051 & -0.1288 \\ & 1.2628 & -0.1288 \\ \text{Symmetric} & & -1.0051 \end{bmatrix} \times 10^3 \text{ lb}$$

$$\begin{bmatrix} D_{11} & D_{12} & D_{16} \\ & D_{22} & D_{26} \\ \text{Symmetric} & & D_{66} \end{bmatrix} = \begin{bmatrix} 7.8844 & 2.8842 & 0.8749 \\ & 9.3791 & 0.6464 \\ \text{Symmetric} & & 3.0057 \end{bmatrix} \times 10^1 \text{ in–lb}$$

The numerical value of the nondimensional orthotropy parameter $\mathcal{O}$ is obtained by substituting the appropriate laminates stiffnesses into equation (20a), which gives $\mathcal{O}$ = 1.0628. To calculate the nondimensional anisotropy parameter $\mathcal{A}_0$, the inverse of the matrix with the subscripted A-terms is needed. This inverse matrix is given by

$$\begin{bmatrix} a_{11} & a_{12} & a_{16} \\ & a_{22} & a_{26} \\ \text{Symmetric} & & a_{66} \end{bmatrix} = \begin{bmatrix} 3.4344 & -1.4604 & -2.2325 \\ & 4.8619 & -0.2400 \\ \text{Symmetric} & & 8.9163 \end{bmatrix} \times 10^{-6} \text{ in/lb}$$

The expressions for a_{12}, a_{22}, and a_{26} are given by equations (C3)–(C5), respectively. Substituting the numerical values for B_{11}, B_{12}, B_{16}, a_{12}, a_{22}, and a_{26} into equation (C6) gives b_{21} = 0.0059 in. Similarly, substituting the laminate stiffnesses into equation (C7) gives $\mathcal{e}_0$ = 0.9713. Next, the values for the laminate stiffnesses, a_{22}, $\mathcal{e}_0$, and b_{21} are substituted into equation (C2) to get $\mathcal{A}_0$ = 1.1940.

The numerical value for the first-order correction factor $\mathcal{C}_1$ is obtained by first substituting the appropriate laminate stiffnesses into equation (C9) to get e_1 = 0.0075. Next, the appropriate laminate stiffnesses are substituted into equations (C14)–(C22); then, the resulting values are substituted into equations (C10)–(C12) to get $a_{112} = 6.2541 \times 10^{-10}$ in/lb, $a_{122} = -1.5760 \times 10^{-9}$ in/lb, and $a_{126} = -5.2861 \times 10^{-9}$ in/lb. Substituting these and the other required values into equation (C13) gives $b_{121} = 3.2255 \times 10^{-5}$ in. Similarly, equation (C8) gives $\mathcal{C}_1$ = 0.0022.

The first-order approximation of the anisotropy factor $\mathcal{A}$ is obtained by substituting the numerical values for μ, $\frac{h}{R}$, $\mathcal{A}_0$, and $\mathcal{C}_1$ into equation (C1). For the present example, $\frac{h}{R} = 0.015$. Substituting the numerical values for the last three of these quantities and μ = 1.5, which corresponds to the use of the Sanders-Koiter equations, into equation (C1) gives $\mathcal{A} = \mathcal{A}_0$ = 1.1940. To compute the exact value of anisotropy factor $\mathcal{A}$ that is given by equation (20b), the laminate stiffnesses, μ, and $\frac{h}{R}$ are substituted in equations (B31)–(B34) to obtain $\bar{A}_{16} = 1.0782 \times 10^5$ lb/in., $\bar{A}_{26} = 0.3927 \times 10^5$ lb/in., $\bar{A}_{66} = 1.3947 \times 10^5$ lb/in., and $\bar{B}_{16} = -1.2555 \times 10^2$ lb. Next, the value for e is computed by substituting these results and the appropriate laminate stiffness values into equation (B49); this action gives e = 0.9714. Then, the quantities defined by equations (B45)–(B48) are calculated to get $\bar{a}_{12} = -1.4604 \times 10^{-6}$ in/lb, $\bar{a}_{22} = 4.8619 \times 10^{-6}$ in/lb, $\bar{a}_{26} = -0.2401 \times 10^{-6}$ in/lb, and $\bar{b}_{21}$ = 0.0059 in. Finally, substituting the appropriate numerical values into equation (20b) gives the exact value of anisotropy factor $\mathcal{A} = \mathcal{A}_0$ = 1.1940, which is identical with the first-order approximation for $\mathcal{A}$.

The nondimensional bending boundary-layer decay length, with anisotropy neglected, is obtained by specifying a value for the tolerance parameter ε and then substituting that value and the numerical value for the nondimensional orthotropy parameter $\mathcal{O}$ into equation (19). For ε = 0.1, this step gives $\frac{d^o}{\sqrt{Rh}} = 1.8595$. This value corresponds to $\frac{d^o}{R} = 0.2277$, which indicates that the bending action attenuates at a distance of approximately 23 percent of the cylinder radius. The nondimensional bending boundary-layer decay length, with anisotropy included, is obtained by substituting the numerical values for $\frac{d^o}{\sqrt{Rh}}$ and $\mathcal{A}$ into equation (18). This step gives $\frac{d}{\sqrt{Rh}} = 2.2202$, which corresponds to $\frac{d}{R} = 0.2719$, which indicates that the bending action attenuates at a distance of approximately 27 percent of the cylinder radius. Overall, these results indicate a very small effect of the laminate anisotropy.

REPORT DOCUMENTATION PAGE

Form Approved
OMB No. 0704-0188

1. AGENCY USE ONLY *(Leave blank)*

2. REPORT DATE
November 2000

3. REPORT TYPE AND DATES COVERED
Technical Publication

4. TITLE AND SUBTITLE
Bending Boundary Layers in Laminated-Composite Circular Cylindrical Shells

5. FUNDING NUMBERS
WU 522-63-31-03

6. AUTHOR(S)
Michael P. Nemeth and Stanley S. Smeltzer, III

7. PERFORMING ORGANIZATION NAME(S) AND ADDRESS(ES)
NASA Langley Research Center
Hampton, VA 23681-2199

8. PERFORMING ORGANIZATION REPORT NUMBER
L-17997

9. SPONSORING/MONITORING AGENCY NAME(S) AND ADDRESS(ES)
National Aeronautics and Space Administration
Washington, DC 20546-0001

10. SPONSORING/MONITORING AGENCY REPORT NUMBER
NASA/TP-2000-210549

11. SUPPLEMENTARY NOTES
Presented at the 41st AIAA/ASME/ASCE/ASC/ASH Structures, Structural Dynamics, and Materials Conference, April 3–6, 2000, Atlanta, Georgia.

12a. DISTRIBUTION/AVAILABILITY STATEMENT
Unclassified–Unlimited
Subject Category 39 Distribution: Standard
Availability: NASA CASI (301) 621-0390

12b. DISTRIBUTION CODE

13. ABSTRACT *(Maximum 200 words)*
A study of the attenuation of bending boundary layers in balanced and unbalanced, symmetrically and unsymmetrically laminated cylindrical shells is presented for nine contemporary material systems. The analysis is based on the linear Sanders-Koiter shell equations and specializations to the Love-Kirchhoff shell equations and Donnell's equations are included. Two nondimensional parameters are identified that characterize the effects of laminate orthotropy and anisotropy on the bending boundary-layer decay length in a very general manner. A substantial number of structural design technology results are presented for a wide range of laminated-composite cylinders. For all laminates considered, the results show that the differences between results obtained with the Sanders-Koiter shell equations, the Love-Kirchhoff shell equations, and Donnell's equations are negligible. The results also show that the effect of anisotropy in the form of coupling between pure bending and twisting has a negligible effect on the size of the bending boundary-layer decay length of the balanced, symmetrically laminated cylinders considered. Moreover, the results show that coupling between the various types of shell anisotropies has a negligible effect on the calculation of the bending boundary-layer decay length in most cases. The results also show that, in some cases, neglecting the shell anisotropy results in underestimating the bending boundary-layer decay length and, in other cases, results in an overestimation.

14. SUBJECT TERMS
Anisotropy; Shells; Edge effects; Cylinders; Decay lengths

15. NUMBER OF PAGES
65

16. PRICE CODE
A04

17. SECURITY CLASSIFICATION OF REPORT
Unclassified

18. SECURITY CLASSIFICATION OF THIS PAGE
Unclassified

19. SECURITY CLASSIFICATION OF ABSTRACT
Unclassified

20. LIMITATION OF ABSTRACT
UL